



TAMPEREEN TEKNILLINEN YLIOPISTO
TAMPERE UNIVERSITY OF TECHNOLOGY

YUCHUAN FAN
MULTITONE NB-IOT OPTIMIZATION BASED ON FILTERED
OFDM WAVEFORM

Master of Science Thesis

Examiner: Prof. Markku Renfors
Examiner and topic approved by the
Faculty Council of the Faculty of
Computing and Electrical Engineer-
ing on 9th August 2017

ABSTRACT

YUCHUAN FAN: Multitone NB-IoT Optimization Based on Filtered OFDM Waveform

Tampere University of Technology

Master of Science Thesis, 56 pages

September 2017

Master's Degree Programme in Electrical Engineering

Major: Wireless Communications

Examiner: Prof. Markku Renfors

Keywords: NB-IoT, filtered-OFDM, uplink, in-band operation mode, filter design, asynchronous multiple access

Narrowband Internet of Things (NB-IoT) is standardized by 3GPP as a novel radio-access scheme for the next-generation IoT technology. In-band operation mode, as one of its deployment methods, shares the spectrum of LTE. To avoid interference leakage on adjacent resource blocks (RBs), the spectrum sharing system needs a spectrally well-localized waveform. In this thesis, we investigate filtered-OFDM waveform for NB-IoT in-band system. This is achieved by designing and exploiting optimized filter for each sub-band. Specifically, the optimum filter needs a suitable length, a relatively narrowed transition band, and adequate stopband attenuation, which efficiently reduces the required guard-band, minimizing the related overhead in resource usage.

In the experiments, we simplify the system model by shifting the NB-IoT RB to the center of the LTE spectrum. Firstly, we test potential filter types with various transition bands, selecting suitable filter configurations with acceptable performance when the system operates under carrier frequency offset (CFO) of half subcarrier spacing. Then, we define two different power level test cases, which are based on the minimum SNR for 1% uncoded bit-error rate (BER), for examining NB-IoT and LTE error tolerance in asynchronous cases, when NB-IoT system fails to synchronize to the time-frequency alignment of LTE. Finally, the system performance in a multipath channel is evaluated. With filtered-OFDM, the out-of-band emission is suppressed effectively and the tolerance to time and frequency offset is significantly improved, which makes the proposed scheme suitable for supporting asynchronous NB-IoT operation.

PREFACE

First and foremost, I am greatly indebted to my supervisor, Prof. Markku Renfors, for his patience, encouragement, and professional instructions during my thesis work. He devotes a considerable portion of his time to weekly meetings, reading my reports and making suggestion for further progress.

In addition, I deeply appreciate my friend and roommate Weijie Zhu for the useful discussions and recommendations of the topic.

I am also grateful to all teaching staff in TUT who once offered me a valuable course and advice during my excellent study journey in Finland. This experience is the most precious memory in my life.

Tampere, 22.9.2017

Yuchuan Fan

CONTENTS

1. INTRODUCTION	1
2. OFDM BASED BROADBAND CELLULAR MOBILE COMMUNICATION SYSTEMS.....	3
2.1 OFDM basics.....	3
2.1.1 Introduction.....	3
2.1.2 LTE numerology.....	5
2.2 5G communications.....	6
2.2.1 Targets, applications and challenges.....	6
2.2.2 Waveform candidates.....	8
2.3 Filtered-OFDM and evolution.....	9
2.3.1 f-OFDM basics.....	9
2.3.2 Filter design aspect.....	10
2.3.3 RB-F-OFDM.....	11
2.3.4 FC-F-OFDM	12
3. INTERNET OF THINGS	14
3.1 Introduction	14
3.2 IoT evolution roadmap	15
3.3 NB-IoT designing features of 3GPP Release 13.....	16
3.3.1 Enhancing indoor coverage.....	16
3.3.2 Improved power efficiency	18
3.3.3 Reduced complexity.....	19
3.3.4 Massive connectivity.....	21
3.4 NB-IoT numerology.....	22
3.4.1 Deployment modes	22
3.4.2 Frame structure	23
4. SYSTEM MODEL.....	25
4.1 Overview	25
4.2 System aspects.....	27
4.2.1 $\pi/2$ -BPSK	27
4.2.2 Transmission end signals and AWGN channel.....	28
4.3 Implementation of Filtered OFDM	31
4.3.1 Symmetrical filtering process	34
4.4 PAPR.....	35
4.5 Matched filtering.....	37
4.6 Equalizer.....	38
4.7 Power level model.....	40
5. RESULTS AND ANALYSIS	42
5.1 AWGN channel testing	42
5.1.1 RRC filter.....	43
5.1.2 Equiripple filter	47

5.2 Veh-A channel testing.....	50
6. CONCLUSION AND FUTURE WORK	53
6.1 Conclusion.....	53
6.2 Future work	53
REFERENCES.....	54

LIST OF SYMBOLS AND ABBREVIATIONS

3GPP	3rd Generation Partnership Project
4G	4th Generation
AWGN	Additive White Gaussian Noise
BPSK	Binary Phase Shift Keying
CFO	Carrier Frequency Offset
CP	Cyclic Prefix
eDRx	extended Discontinuous Reception
eMBB	enhanced Mobile BroadBand
eMTC	enhanced Machine-Type Communication
FBMC	Filter Bank Multicarrier
FFT	Fast Fourier Transform
f-OFDM	Filtered OFDM
GSM	Global System for Mobile Communications
H-FDD	Half Frequency Division Duplex
ICT	Information and Communications Technology
ISI	Inter-Symbol Interference
IoT	Internet of Things
LPWA	Low Power Wide Area
LTE	Long Term Evolution
MIMO	Multi-Input Multi-Output
OFDM	Orthogonal Frequency-Division Multiplexing
OOBE	Out-Of-Band Emission
PA	Power Amplifier
PAPR	Peak to Average Power Ratio
PRB	Physical Resource Block
PSD	Power Spectrum Density
PSM	Power Saving Mode
QAM	Quadrature Amplitude Modulation
QPSK	Quadrature Phase Shift Keying
RRC filter	Root Raised Cosine filter
SC-FDMA	Single Carrier Frequency Division Multiple Access
TO	Timing Offset
UFMC	Universal Filtered Multicarrier

1. INTRODUCTION

During the past few decades, wireless communication systems have progressed rapidly. With the ever-growing number of users, our lives have changed widely by the fourth generation (4G) mobile communication system called LTE (long term evolution). While human-to-human mobile communications are expanding with new services and applications, also machine-to-machine type communications are expected to be deployed widely. Everything connecting will be an inevitable trend and enable various novel application scenarios for the next generation communication system. The Internet-of-things (IoT) has become an important innovation engine for the ICT industry, and more and more innovative and promising IoT applications are expected to be deployed through 4G (and later 5G) networks, including the logistics market, vehicle communications, remote medical service, and so on. Existing IoT devices utilize a local wireless network to establish connections to each other, which severely limits the availability of IoT services to mobile users. [1]

To increase the IoT devices' mobility and connection quality, and enjoy current mobile cellular network connections, 3rd generation partnership project (3GPP) introduced a new radio access technology, namely Narrowband Internet of Things (NB-IoT). According to the spectral localization of a NB-IoT physical resource block (PRB), three different operation modes can be defined: in-band, guard-band and stand-alone. NB-IoT system can either occupy 1 PRB of LTE resources in the in-band option, or make of the guard-band of LTE as transmission resource in the guard-band option. In case of stand-alone option, NB-IoT could be deployed on a reframed GSM carrier, also called EC-GSM-IoT. In this thesis work, we mainly consider enhancement of the in-band operation mode. [2][3][4]

In Release 13, NB-IoT in-band operation is based on 4G LTE framework, which keeps most of LTE features and takes advantage of the LTE infrastructure. The underlying waveform of NB-IoT adopts orthogonal frequency-division multiplexing (OFDM). OFDM enables LTE systems to benefit from high spectrum utilization efficiency, high data rate, and robustness to multipath propagation environment, etc. [3]

Although the OFDM waveform has many advantages for LTE system, it suffers several crucial problems [5]. The main drawback is the case that OFDM waveform contains high out-of-band emission (OOBE), which is due to IFFT processing of OFDM modulation. The in-band operation mode has NB-IoT and LTE in different sub-bands, and NB-IoT occupies one PRB within the LTE spectrum resources. If one of them loses synchronization, high side lobe power will leak into adjacent user equipment (UEs), causing adjacent edge users of NB-IoT and LTE to interfere with each other. On the other hand, OFDM

system is very sensitive to the timing offset (TO) and carrier frequency offset (CFO), these offsets are prone to appear in the two sub-band signals superposition process. Both timing offset and frequency offset would destroy the orthogonality of the subcarriers. All of these would reduce the performance of the system. The limited in-band spectrum resources motivated us to re-examine the underlying waveform. [6][7][8]

In this thesis, filtered-OFDM waveform, a promising 5G waveform candidate, is investigated in the in-band operation mode. To facilitate a simplified simulation model of the filtered waveforms for NB-IoT and LTE sub-bands, we make a slight equivalent change to the in-band signal model. By symmetrically shifting the PRB of NB-IoT to center of LTE spectrum, we can simulate the filtered system performance with a simple FIR low-pass and high-pass filter for NB-IoT and LTE, respectively. In our experiments, we firstly tested various potential filter types suggested by Huawei research, such as different window function types and equal-ripple filter. By comparing these filter types, root-raised-cosine (RRC) filter and equal-ripple filter emerged as a narrow transition bandwidth filter designs of distinction. We defined optimum and critical power control scenarios, which was based on the required SNR for 1% uncoded bit-error-rate (BER). Then, we selected RRC and equal-ripple filter designs with mixed filter configuration to examine the filtered system error tolerance in imperfect synchronization and non-ideal power control scenarios. Finally, we validated the capability of our filtered system by simulations in a wireless propagation environment including a frequency-selective multipath channel model.

The remaining chapters of the thesis are organized as follows. The principles and the background of the OFDM, LTE, and 5G waveform candidates are provided in Chapter 2. Chapter 3 introduces the theoretical background of IoT, including existing IoT systems and the emerging 3GPP cellular IoT technology. Our system model and specific simulation configurations are discussed in Chapter 4. After that, the experimental results are presented and evaluated in Chapter 5. Finally, the main conclusions and potential future work are summarized in Chapter 6.

2. OFDM BASED BROADBAND CELLULAR MOBILE COMMUNICATION SYSTEMS

2.1 OFDM basics

2.1.1 Introduction

In 1960s, the birth of multicarrier communication systems was realized, but for a long while, its complexity was too high for commercial deployment and it was mainly considered for military applications. Subsequently, researchers actively explored ways to reduce its complexity. Finally, in 1971, Weinstein and Ebert first discovered that Fast Fourier Transform (FFT) would be able to implement multicarrier modulation and demodulation effectively, and the FFT-based scheme was named as OFDM. They introduced also the idea of guard interval to deal with multipath transmission channels. However, the use of the guard interval with multipath channel destroys the orthogonality between subcarriers and greatly damages the performance of such OFDM schemes. In 1980, cyclic prefix (CP) was proposed as an ideal protection interval scheme. Later, the FFT based CP-OFDM hardware system was implemented and widely used as the basis for various wireless communication systems. [9]

The fourth generation (4G) communication system, also called long term evolution (LTE), which services as mainly communication standard all over the world. 3GPP formulates the physical layer transmission scheme in LTE system, which is OFDM access (OFDMA) and single carrier frequency division multiple access (SC-FDMA) in downlink and uplink respectively [10]. A simple baseband OFDM/SC-FDMA transceiver is shown in Figure 2.1.

OFDM is a special multi-carrier transmission scheme, which can be regarded as a modulation technique or a multiplexing technique. Because of its technical maturity, it was proposed as the downlink standard for LTE and a consensus on this choice was soon reached. Regarding the choice of uplink technology, due to the high PAPR of OFDM, some equipment vendors thought it will increase the terminal power amplifier cost and power consumption, limiting the terminal battery lifetime. After discussions, the SC-FDMA with low PAPR characteristics was adopted for the uplink transmission.

The main idea of OFDM is that the transmitter converts a serial high rate data stream into multiple parallel low-speed sub-data streams by means of serial to parallel conversion. Each sub-data stream uses traditional modulation schemes for low symbol rate modulation, such as phase shift keying (PSK) or Quadrature Amplitude Modulation (QAM), which transforms bits into symbol streams. Then, the symbol streams are mapped into

different orthogonal subcarriers. The raw serial data can be obtained by performing the reverse process at the receiver side, as shown in Figure 2.1. [9]

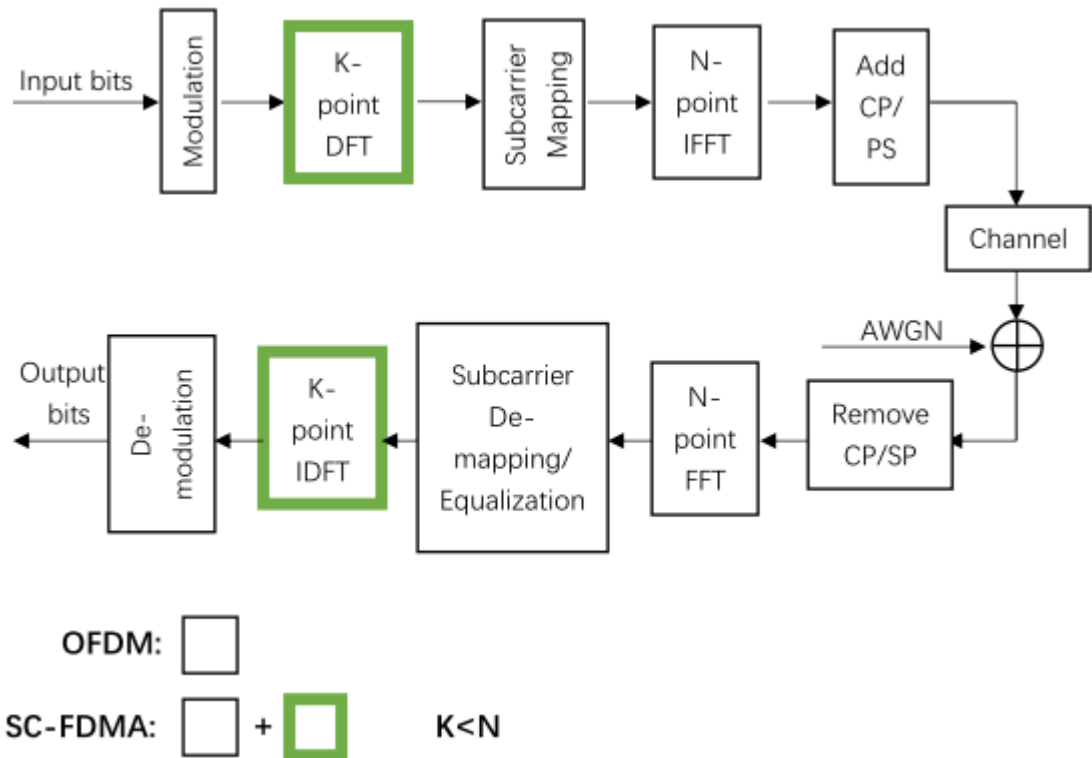


Figure 2.1 Baseband OFDM/SC-FDMA transceiver block diagram.

OFDM has many benefits as the waveform standard of LTE [11]:

1. Low speed parallel transmission: High-speed serial data flows through serial-to-parallel conversion, divided into several low-speed parallel data streams, and each parallel data stream adopts independent carrier modulation. The orthogonality between sub-carrier helps to avoid interference, and the spectrum utilization is greatly improved because subcarriers are packed with maximum spectral-density.
2. Anti-fading and equalization: Each channel occupies a relatively narrow channel bandwidth due to the division of the channel band by the OFDM, so it can be considered as a flat fading channel. In this way, OFDM technology has the characteristics of anti-fading of the large bandwidth system and simple equalization of small bandwidth sub-carriers.
3. Robustness to Inter-symbol interference (ISI) of multipath delay: In OFDM technique, cyclic prefix (CP) can be introduced so that ISI can be efficiently eliminated as long as the time interval of CP is longer than the channel delay spread. under these conditions, the flat-fading subcarrier model applies precisely.
4. Adaptive multi-user scheduling: OFDM system can use frequency selectivity of channel for multi-user scheduling, and users' data streams can be scheduled on the best frequency-domain resources for data transmission, thus obtaining multi-user diversity gain in frequency-domain scheduling.

5. DFT based implementation: Discrete Fourier Transform (DFT) can be used for modulation and demodulation of OFDM signals, thus solving the technical problems of OFDM implementation. In practical applications, the Fast Fourier Transform (FFT) and its inverse transform (IFFT) are often used in practice to realize the modulation and demodulation of OFDM.

However, the CP insertion will decrease the spectrum efficiency and data rate. In addition, possible carrier frequency offset (CFO) and timing offset (TO) have significant effects on OFDM transmission, which result in system power loss and ICI/ISI. Strict time-frequency alignment is required to ensure correct demodulation. Undoubtedly, this will lead to significant signaling overhead. Moreover, high peak to average power ratio (PAPR) more easily causes nonlinear distortion in transmitter power amplifier, which makes mobile devices transmitter power amplifier design challenging.

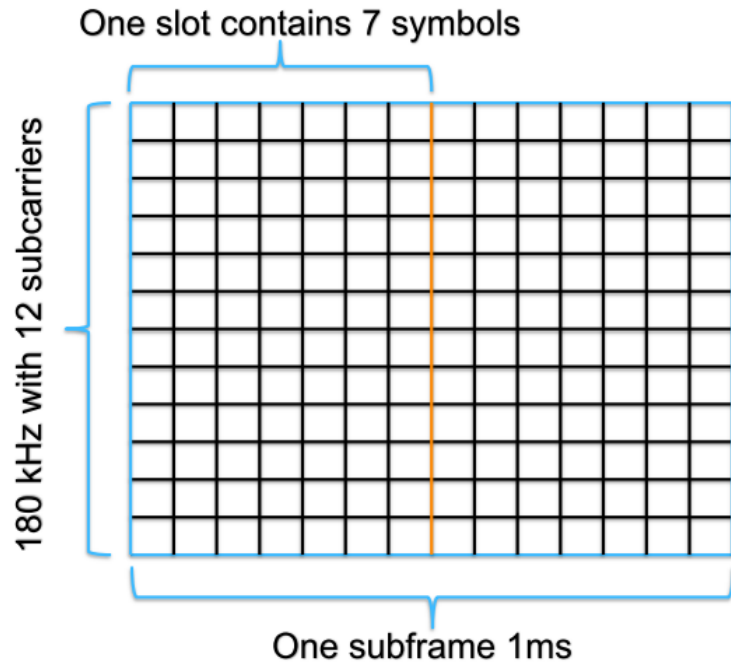
The OFDM output sample sequence after IFFT processing, $x(k)$, can be written as:

$$x(k) = \frac{1}{N} \sum_{i=0}^{N-1} X(i) e^{j2\pi ki/N}, \quad (2.1)$$

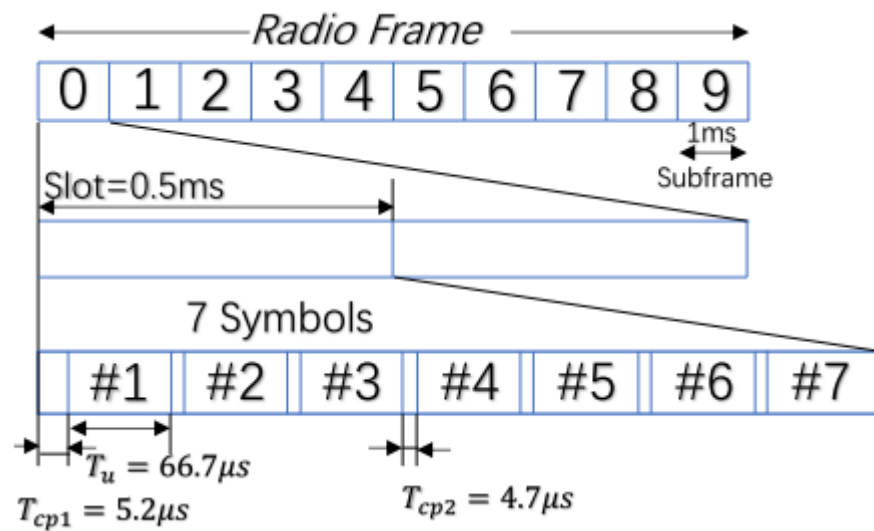
where N denotes the IFFT length and $X(i)$ is the symbol modulated to subcarriers i . From this equation, we can see that a single sample consists of the summation of all symbols, each multiplied by a phasor term. This summation leads to PAPR that is proportional to N , in the worst case. In contrast, SC-FDMA has lower PAPR. Its basic principle is similar to OFDM, only a DFT module is added before the sub-carrier mapping. The modulated data symbols are converted into frequency-domain, in other words, the single symbol information is extended to all the sub-carriers, and each sub-carrier depends on all the information symbols. Therefore, SC-FDMA is also known as the DFT-spread-OFDM.

2.1.2 LTE numerology

Basically, in time domain, 1 subframe means 1 ms, which contains 2 slots. Subframe provides the absolute time reference, independently of the selected numerology. Slot is a fundamental scheduling unit: 1 slot contains 7 OFDM symbols. On the other hand, in frequency domain, the main-lobe of each OFDM subcarrier is 15 kHz wide, and the sub-carrier spacing is 15 kHz. 12 subcarriers and 1 slot compose 1 physical resource block (PRB), which is the fundamental unit of LTE air interface allocation. Besides, the alternative LTE channel bandwidths are 1.4 MHz, 3 MHz, 5 MHz, 10 MHz, 15 MHz, 20 MHz, corresponding to 6, 15, 25, 50, 75, 100 PRBs, respectively. Figure 2.2 illustrates a typical LTE frame structure in time-frequency domain. [18]



(a)



(b)

Figure 2.2 (a) LTE PRB/subframe structure, (b) LTE time domain frame structure with CPs.

2.2 5G communications

2.2.1 Targets, applications and challenges

The next generation cellular mobile communication scheme is a hot topic in this realm, for which a clear target has been established after years of discussion. In general, the

consensus on 5G cellular network characteristics is high capacity, low latency, high reliability, massive connectivity and low power consumption. Naturally, it is not reasonable to assume all these characteristics for all kind of services. Therefore, 5G is going to offer three major different types of major application scenarios: enhanced mobile broadband (eMBB), massive machine type communication (mMTC), ultra-reliable and low latency communications (URLLC) [5]. Specific usage examples are illustrated in Figure 2.3.

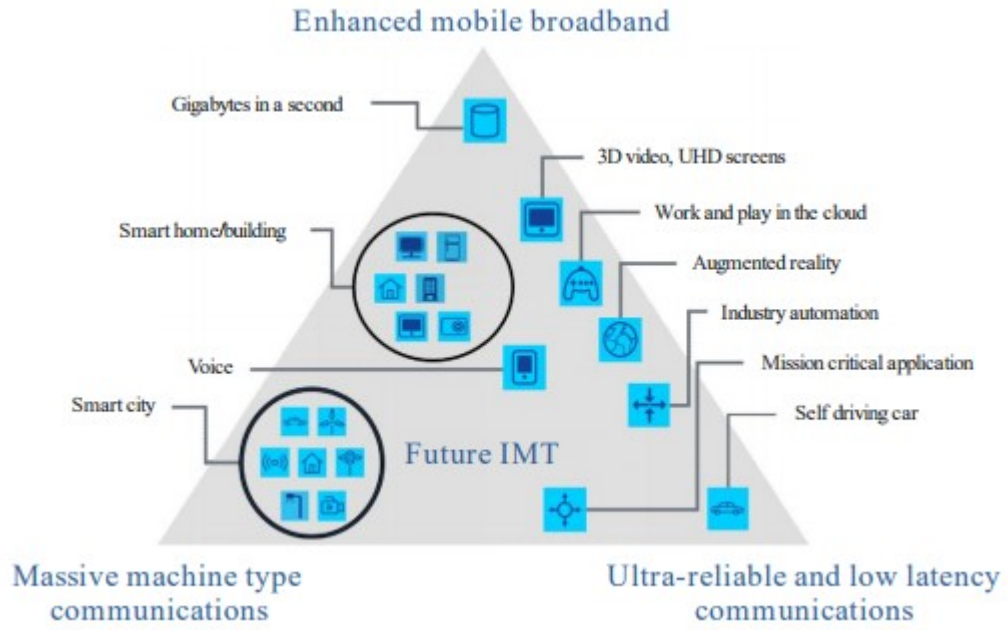


Figure 2.3 Future applications of 5G. [5]

Additionally, 5G has a variety of scenario and usage requirements, which demands a fusion of multiple wireless access schemes to ensure effective use of limited spectrum resources. Thus, the next generation communication standard will support multiple OFDM numerologies. In addition to 15 kHz subcarrier spacing, it enables 15×2^n kHz scenarios. For instance, 30/60 kHz is available to dense-urban, lower latency and wider carrier bandwidth; 60 kHz or higher is used against phase noise in the frequency band over 10 GHz; conventional 15 kHz supports the traditional wide area cellular band. Since various subcarrier spacings are adopted, the slot structure changes and becomes more complicated. The minimum slot length contains 7 OFDM symbols for subcarrier spacing smaller than 60 kHz. Instead, the slot for subcarrier spacings greater than 60 kHz is composed of 14 symbols.

Generally speaking, 5G air interface roadmap contains both revolutionary and evolutionary elements. The former includes various key techniques to meet the future requirements, such as massive multi-input multi-output (massive MIMO) multiantenna techniques, full-duplex transmission, software defined cloud-based network elements, etc. The latter consists of LTE enhancement, exploiting existing infrastructures. Moreover, after extensive research efforts to develop new waveform solution for 5G, there is a tentative decision to

use CP-OFDM with options to use spectrum enhancement techniques, e.g., based on filtering or time-domain windowing. Figure 2.4 shows the essential physical layer blocks in each generation of wireless communication technology, as well as possible candidates for each block in 5G. [5]

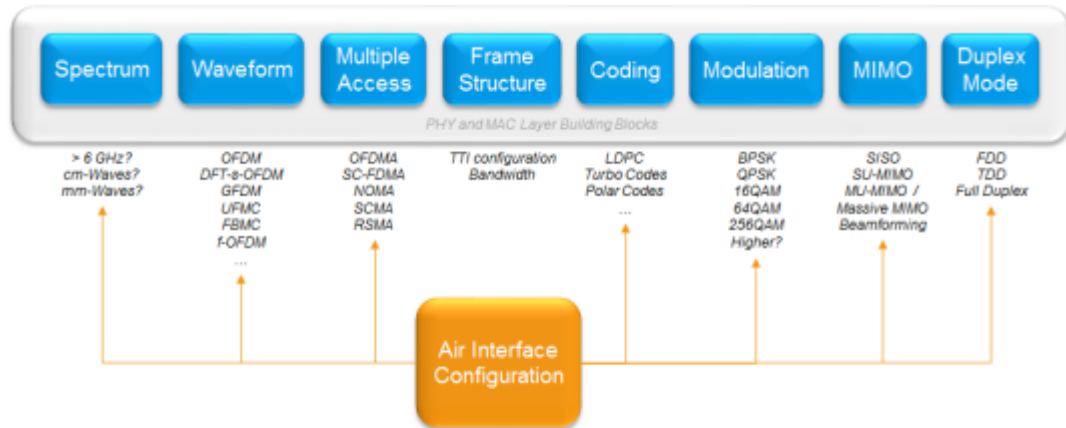


Figure 2.4 5G new air interface configuration and alternative technologies. [5]

2.2.2 Waveform candidates

Waveform technique is the key physical layer fundamental. OFDM brings us high transmission efficiency, easy implementation, and convenient application of various multi-antenna transmission with many benefits. However, Internet of things, machine type communication and tactile network will have an important position in the future communication system, which evoke new requirements for the spectral characteristics, system delay, power consumption, and synchronization. Conventional OFDM suffers from serious limitations of high out-of-band emission (OOBE), stringent synchronization requirements, and only one waveform configuration in the whole channel. Thus, to satisfy the diverse requirements, the underlying waveform should be revisited. [6]

The new waveform should be able to dynamically adapt to different application scenarios, by selecting and configuring waveform parameters, whilst coexisting with conventional CP-OFDM. In addition, 5G system will enable massive communication of IoT sensors, and most of sensor devices perform irregularly communication with low data rate. On the other hand, if IoT sensors utilize the LTE system, the current random-access mechanism will produce a lot of signaling overhead, and closed-loop time synchronization will consume a lot of energy, shortening the terminal equipment battery life. Therefore, 5G waveform candidate should be capable of supporting asynchronous transmission to reduce signaling overhead and energy consumption of the system. [5]

Currently, the 3GPP baseline assumption of the waveform for below 40 GHz communications is CP-OFDM, possibly with additional spectrum enhancement methods. These include time-domain windowing methods, referred to as weighted overlap and add

(WOLA). A family of alternative schemes, generally considered to be more effective but also more complicated, are referred to as filtered OFDM (f-OFDM). [36]

This thesis work mainly studies the most promising waveform f-OFDM, which used for optimizing the in-band NB-IoT capability.

2.3 Filtered-OFDM and evolution

2.3.1 f-OFDM basics

To overcome the limitation of OFDM, f-OFDM is suggested by Zhang *et al.* [6], and Abdoli *et al.* [7]. In this variant of OFDM, the system bandwidth is divided into a number of sub-band, and together with sub-band-wise bandpass filtering, the scheme can support asynchronous transmission. Figure 2.5 depicts an asynchronous uplink transmission scheme based on filtered-OFDMA/filtered-SC-FDMA. On the UE side, there is a spectrum shaping filter $f_i(n)$, which corresponds to the bandwidth of the active subcarriers. On the other side, the BS performs a matched filtering process $f_i^*(-n)$ on the received signal to eliminate the interference from the other sub-bands. Moreover, each sub-band can deploy different configuration parameters for specific applications. The filtering process makes the signal to have a very low out-of-band spectrum leakage so that the f-OFDM system can use fragmented spectral portions and the spectrum efficiency is improved because a very low number of guard tones is sufficient between sub-bands [6][7].

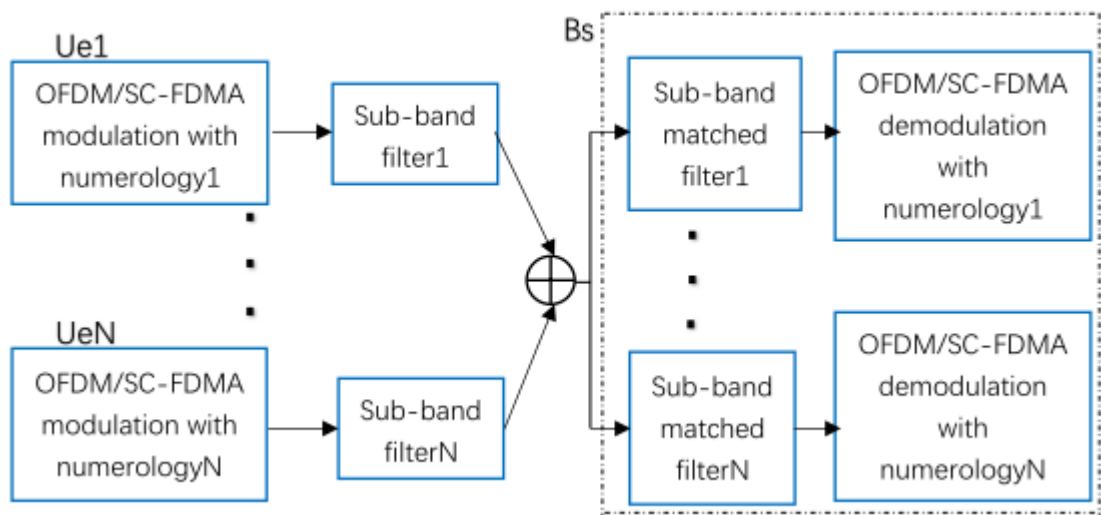


Figure 2.5 UE to BS asynchronous filtered-OFDMA/filtered-SC-FDMA.

An example of the PRB configuration of f-OFDM with mixed numerology is illustrated as Figure 2.6. We can see that the symbol duration (together with subcarrier spacing) can be flexibly assigned. There is no requirement for orthogonality among the subcarriers of different sub-bands, because filtering suppresses interference leakage between them.

However, we need to introduce guard bands to ensure sufficient interference rejection. LTE system uses 10% bandwidth as guard band. Through the filter design, the guard band between adjacent sub-bands can be reduced to one or few subcarrier spacings, depending on the acceptable level of crosstalk.

Regarding the f-OFDM evolution, Li *et al.* [8] proposed a non-continuous way to apply the filtering process in spectrum fragments, named resource block filtered OFDM (RB-F-OFDM), which efficiently exploits discontinuous spectrum fragmentation. Moreover, the work published by Renfors *et al.* [12] showed that the resource block f-OFDM technique can be effectively realized by the fast convolution filtering scheme, which is less complex and more flexible than time domain filtering.

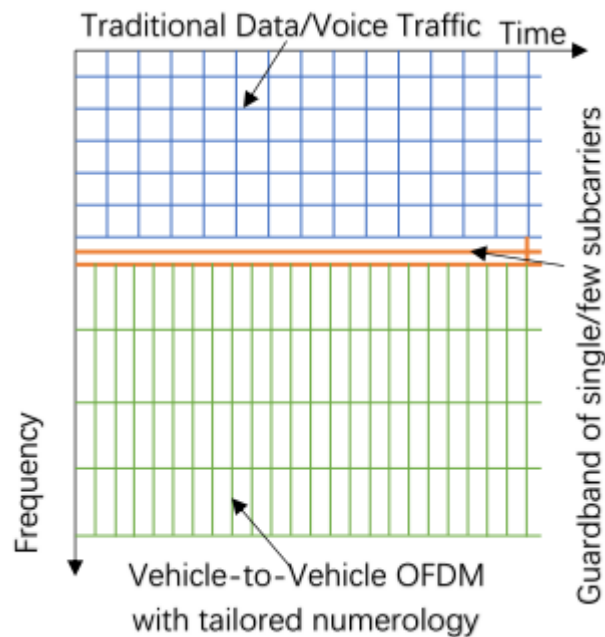


Figure 2.6 Example of F-OFDM PRB partitioning to different sub-bands with different numerologies according to different service requirements.

2.3.2 Filter design aspect

Filter parameter selection will have a significant impact on the system. These parameters include passband ripple, transition bandwidth, stopband ripple, and filter length. Among them, the passband ripple and stopband ripple influence on the frequency spectrum of the signal. The OFDM channel equalizer is able to compensate minor imperfections of the passband response. The stopband attenuation should be sufficient to reduce the interference leakage to an acceptable level, but generally modest stopband attenuation (say 20-40 dB) is sufficient for this purpose. Therefore, these characteristics are not in the focus of optimal filter design for this application. The transition band should be as steep as possible to minimize the width of the guard band, which should be proportional to the filter transition bandwidth. By not using the subcarriers that fall on the filter transition

band, together with sufficient stopband attenuation, we ensure the suppression of interference leakage to adjacent sub-band signals in case of asynchronous or mixed numerology transmission. Minimizing the guard bands enhances the spectrum utilization efficiency. On the other hand, the filter length determines the time-domain tailing of signal. Obviously, long signal tailing will introduce ISI. Thus, the filter parameter selection needs to consider the tradeoff between the filter length and frequency domain characteristics. Therefore, in order to guarantee good system performance, the filter should be rationally designed such that all parameters meet the system requirements. [6][7][8][12]

Filter design is the core part of f-OFDM technique. Generally, only finite impulse response (FIR) filters are considered for this application. There are three basic approaches for FIR optimization [6], windowed sinc method, equiripple method, and Raised-cosine filter:

- Windowed sinc method: The frequency response of an ideal filter is rectangular, which can perfectly filter the signal, but the corresponding time domain sequence $f_d(n)$ is non-causal and has infinite length. Window based FIR filter design utilizes different window functions $w(n)$, such as Hann window, Hamming window, etc., to truncate the ideal low pass impulse response (also known as sinc function) $f_d(n)$. Then, the filter time domain response $f(n)$ can be written as the convolution of $f_d(n)$ and $w(n)$ [6][7]:

$$f(n) = w(n) \cdot f_d(n), \quad (2.2)$$
- Equiripple method: This type of filter design utilizes the Remez exchange algorithm, which can minimize the transition bandwidth for given stopband attenuation and passband ripple specifications, further reducing the interference between sub-bands. But the impulse response of the resulting filter is discontinuous at both ends. Consequently, the time-domain characteristics of these filters are not so good. In addition, the Remez exchange algorithm is rather complicated and cannot generate filters online. [6]
- Raised-cosine (RC) and root-raised-cosine (RRC) filters are commonly used in communications signal processing for pulse shaping and also for various other purposes. These filters are defined in the frequency domain, with the transition bandwidth (or roll-off) as the single design parameter. These filters have also infinite and non-causal impulse responses and need to be truncated to a finite length by a window function, which in the simplest case could be a rectangular window cutting the impulse response symmetrically to a finite length.

2.3.3 RB-F-OFDM

Basically, resource block filtered-OFDM (RB-F-OFDM) implements the filtering process per-PRB, which enables the exploitation of different spectrum types, such as contiguous and non-contiguous, and the dynamic design of filters for each fragment. RB-F-OFDM takes advantage of polyphase filter banks and f-OFDM, by dividing the available spectrum fragments into resource blocks (see Figure 2.7). This can be done in a compatible way with existing OFDM systems, for instance, the RB-F-OFDM receivers can also demodulate OFDM signals. Figure 2.8 depicts the RB-F-OFDM transceiver block diagram, which

contains a phase rotation unit to reduce PAPR of system. Assuming B sub-bands contain the N available subcarriers, RB-F-OFDM generates $S_i(n)$ by a smaller OFDM transmitter, with a R -point IFFT. This signal is filtered with a FIR low pass filter after $Q = N/R$ up-sampling process. RB-F-OFDM presents a delightful performance regarding the OOB and adjacent channel interference rejection over f-OFDM. [8][32]

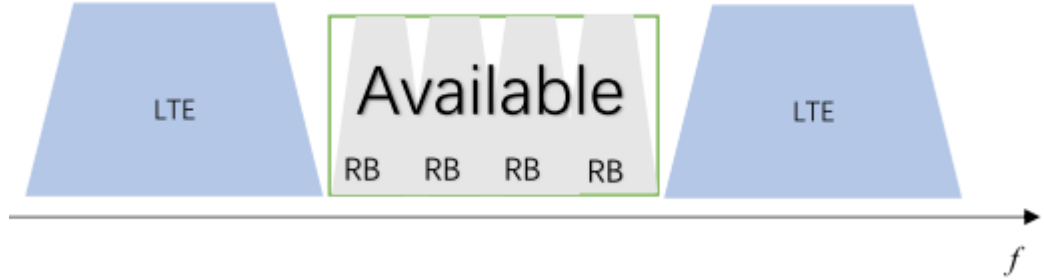


Figure 2.7 Non-contiguous spectrum divided into RBs.

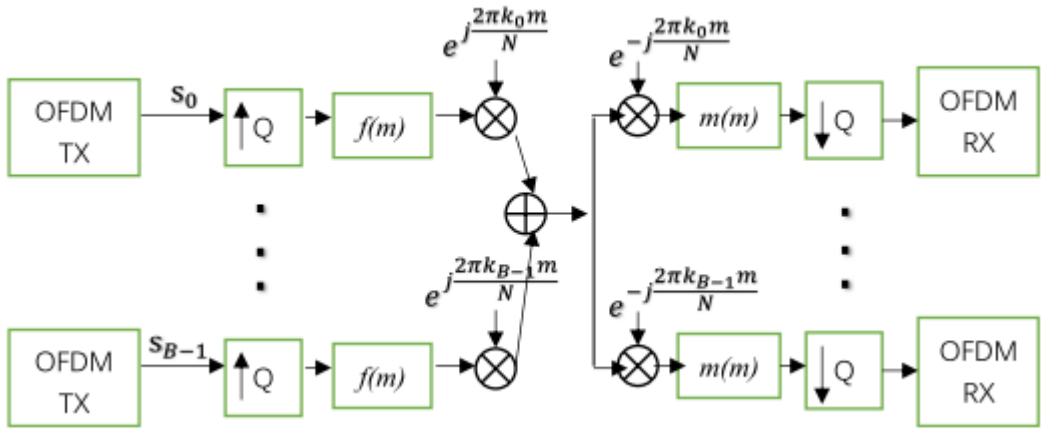


Figure 2.8 RB-F-OFDM transmitter and receiver block diagram.

2.3.4 FC-F-OFDM

To boost the implementation efficiency of high-order filters, Renfors *et al.* [12] proposed a novel scheme, which is named as fast convolution filtered OFDM (FC-F-OFDM). The idea comes from the idea that multiplication in FFT-domain can effectively implement a long impulse response linear FIR filter. Besides, increasing the overlap factor can eliminate the inherent cyclic distortion effect with affordable computational complexity. The frequency response is determined by transition band weights in FFT-domain and the same weights can be used for filters with different bandwidths through extending the passband with unity-valued weights. Therefore, we can design FC filter in FFT-domain by optimizing the weight coefficients.

Consequently, compared with the time-domain filter, FC-F-OFDM method has straightforward implementation and it is more flexible. Additionally, this scheme enables either contiguous synchronous or asynchronously resource blocks operation. On the one hand, for asynchronously resource blocks, the interference leakage between resource blocks can be suppressed effectively. On the other hand, operation of contiguous synchronous resource blocks can implement without filtering guard-bands. [12]

3. INTERNET OF THINGS

3.1 Introduction

The world is in the intersection of the physical world and the virtual world. Human-to-human, human-to-things, and things-to-things are forming ubiquitous connections. Internet of things (IoT) is an important revolution in the information age, which is aimed at realizing the connection of everything. This is essential for the construction of the smart cities. Based on the ubiquitous cellular communication network, IoT technology can be used as variety of wireless communication solutions in a wide range of fields, such as remote meter reading, intelligent transportation, security monitoring and asset tracking, etc. Many market prospects indicate that the M2M connections will have an explosive growth in the following few years. Figure 3.1 is a vision provided by Cisco VNI Mobile, 2017.



Figure 3.1 M2M device connections forecast. [13]

We can classify the IoT techniques based on coverage and network quality as indicated in Figure 3.2. [13]

1. Horizontal axis: It can be defined as short vs. long distance coverage. Short distance techniques include WiFi, Bluetooth and ZigBee, etc. However, those short distance techniques are inherently limited by the coverage inherently, which accordingly restricts application scenarios. For example, remote measurement systems are usually placed in a basement or an out-of-the-way place, which requires high coverage capability. Regarding long distance communication, the main representative techniques are NB-IoT, eMTC, LoRa, and SigFox. They are characterized by wide coverage, low cost, low power, and massive connection. We also call this type of technology as Low Power Wide Area (LPWA).
2. Vertical axis: It can be divided into low, medium, and high data rate levels. Low data rate (<200 kbps) refers to NB-IoT, LoRa, Sigfox, Bluetooth, ZigBee, etc. short-range technologies, with main application scenarios like utility meters, meteorological / environmental monitoring, intelligent lock, intelligent parking. Medium data rate (<1 Mbps), techniques include eMTC, GPRS/CDMA, WiFi, etc., and they have application areas like wearable equipment, banking point of sale

(POS) devices, fleet management, etc. High data rate includes vehicle networking, video monitoring, remote surgery, etc. These scenarios, which need over 1 Mbps data rate and are served mainly by 4G LTE and 5G techniques.

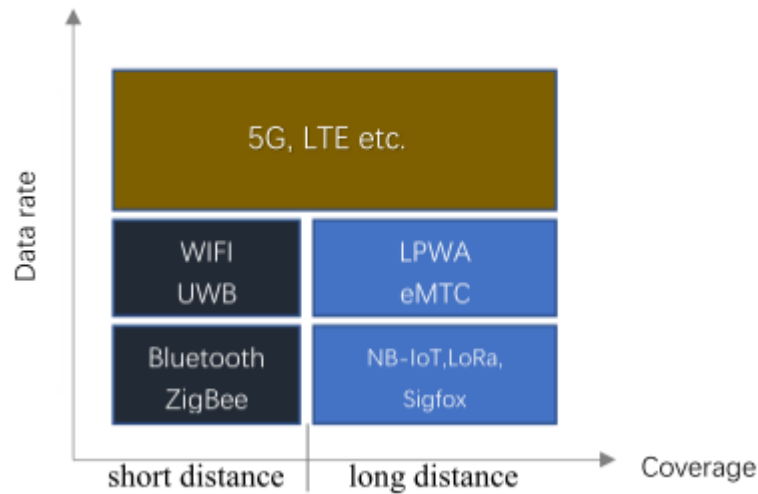


Figure 3.2 Different IoT techniques

LPWA IoT networks can generally be classified into unlicensed networks and evolution of 3GPP licensed networks. Unlicensed networks, including LoRa and SigFox, mostly are nonstandard and custom implemented. Those schemes operate mostly in ISM (Industrial Scientific Medical) band and have been deployed in numerous fields. On the other hand, 3GPP licensed networks, like NB-IoT and eMTC, are evolving with existing cellular networks and bring potential business opportunities for mobile operators. [15]

3.2 IoT evolution roadmap

At present, the existing IoT applications supported by 2/3/4G suffer from several drawbacks:

- Inadequate coverage for typical application scenarios, for instance: indoor wireless meter reading, remote area environmental monitoring, underground resource monitoring, etc.
- Excessive terminal power consumption.
- 2/3/4G cannot meet the demands of the future massive terminal deployment.
- High overall cost, considering communication module and application development.

This motivates the development of new cellular IoT schemes. Figure 3.3 illustrates different steps in the cellular IoT evolution. As we can see from the roadmap, there are two major factions within the 3GPP solution of the Internet of things. One is the eMTC technology based on LTE network adaptation for these applications, and the other is the new NB-IoT technology. Moreover, 3GPP defines different configuration requirements for different users. The Cat-NB1 has the simplest structure and discards the voice communications to reduce the cost and complexity of terminals. The relationship between NB-IoT

and eMTC is a long-term coexistence, because the market positioning is different, eMTC is for medium-rate IoT demand, and NB-IoT to solve the low-rate demand. [16] [17]

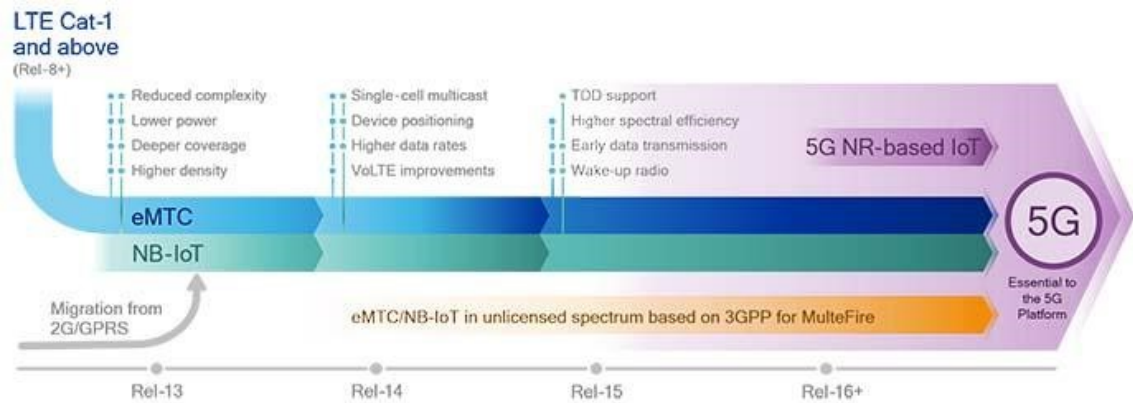


Figure 3.3 Cellular IoT schemes evolution roadmap. [17]

3.3 NB-IoT designing features of 3GPP Release 13

NB-IoT is included in 3GPP Release 13 as a new Internet of things wireless access technology. As a low-power wide-area wireless access technique, NB-IoT has the advantages of wide coverage, massive connectivity, low power consumption, and low cost [3][19].

- Coverage: Compared to the traditional global mobile communication system (GSM) network, NB-IoT can provide 20 dB coverage gain, and its link budget reaches -164 dB;
- Connecting: NB-IoT can support 5~10 million devices per sector;
- Low power consumption: NB-IoT Internet of things terminals, according to different business models, have up to 10 years life cycle;
- Low cost: The cost of the NB-IoT module is expected to be around \$5, which has significant cost advantages compared to a 3G/4G module.

3.3.1 Enhancing indoor coverage

The existing IoT equipment suffer from network coverage problems, for example, a utility meter is often placed in a deep basement. Compared with a typical smart phone case, the height difference results in a 4 dB attenuation, and the lid of the equipment will have 10 dB additional attenuation. Thus, the 3GPP has set a coverage target (see Table 3.1), which extends 20 dB over the existing commercial GPRS devices. This target can be achieved by: 1. Improving power spectrum density (PSD), 2. Using repeated transmissions, 3. Deploying at low frequency band. [26]

Table 3.1 3GPP specifications for the maximum coupling loss (MCL). With the new standard, a Cat-M1 device link budget improves to 156 dB, which is a +11 dB improvement over conventional LTE. Besides, Cat-NB1 is further increased to 164 dB.

Type	Uplink (dB)	Downlink (dB)
GSM/GPRS	-144	-149
Broadband LTE	-144	-150
LTE-M (eMTC)	-156	-156
NB-IoT	-164	-164

1.Improving PSD

Reducing the transmission bandwidth enhances the power spectral density of IoT terminals, as presented in Table 3.2. Under the same transmission power, a single-tone NB-IoT transmission has 12 times higher PSD over a typical GPRS equipment. This corresponds to $10 * \log(12) = 11$ decibels. Single-tone NB-IoT and 2G/3G/4G IoT uplink bandwidths are 3.75/15 kHz and 180 kHz (without guard-band), respectively. Hence in NB-IoT, a unit bandwidth carries more energy than that in 2G/3G/4G, providing higher SNR at receiver, and it can cover a longer distance.

Table 3.2 PSD comparison between a NB-IoT and typical GPRS equipment in the same frequency.

Type	Power (mW)	Bandwidth (kHz)	PSD=Power/Bandwidth (mW/kHz)	Ratio
NB-IoT	200	15	13.33	12
GPRS	200	180	1.11	

2.Repetitive transitions

NB-IoT obtains time diversity gain by repeating transmission, and adopts low order modulation to improve demodulation performance and enhance coverage. This mechanism is like the case where we cannot easily hear the message at once, and we can repeat the message several times, which increases the probability to be heard. In the 3GPP standard, all physical channels can apply repetitions, providing gains of 3-12 dB in theory (see Figure 3.4) [20]. Nevertheless, the transmission rate drops by half when we repeat the message once, while the coverage increased by 3 dB. The maximum uplink repetition is 128 times, but considering the rate of cell edge scenario and data channel capacity, uplink retransmissions are limit to 16 times, corresponding to 12 dB actual gain.

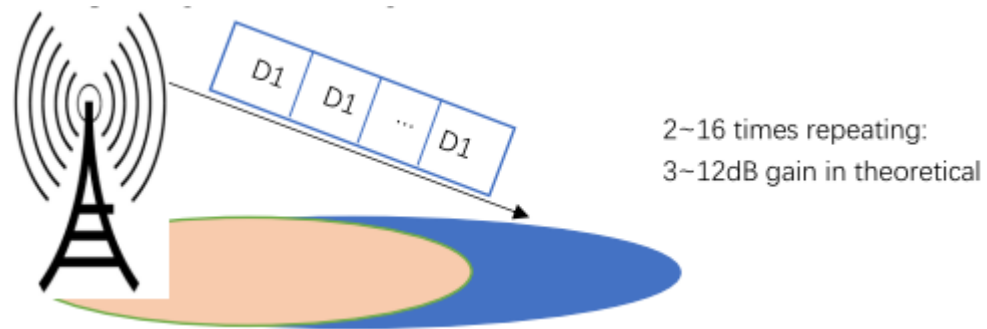


Figure 3.4 Data retransmission model

3. Deploying in low frequency band

Although NB-IoT can be assigned to any frequency band, but considering coverage requirements, generally, below 1 GHz is selected for its deployment [21]. Compared with high frequency, low frequency has the advantages of lower path loss and stronger diffraction ability, which are more suitable for long-distance coverage.

By those schemes, we can ensure the 20 dB gain for NB-IoT, even if GPRS devices using the maximum transmission power 2000 mW (10 dBm higher than NB-IoT), we can utilize 3.75 kHz subcarrier spacing and increased number of retransmission to compensate the power difference.

3.3.2 Improved power efficiency

NB-IoT devices are mostly battery-powered, and a long battery life is very desirable. Especially in massive deployments, battery changing would be a huge overhead compared to the economic benefits it can bring. Thus, 3GPP has set the long battery life as one of the main improvement target. There are two new low-power schemes for cellular IoT devices adopted by 3GPP: power saving mode (PSM) and extended discontinuous reception (eDRx). [3][19]

Power Saving Mode: IoT devices are different from mobile phones, which might just report one or two messages per day or week. Thus, it's possible to stay a long time asleep, instead of monitoring the network at all times, reducing power consumption of RF and signal processing, etc. PSM technology (see Figure 3.5) is introduced in Release 12, which allows the devices to remaining registered in the network while in the PSM state.

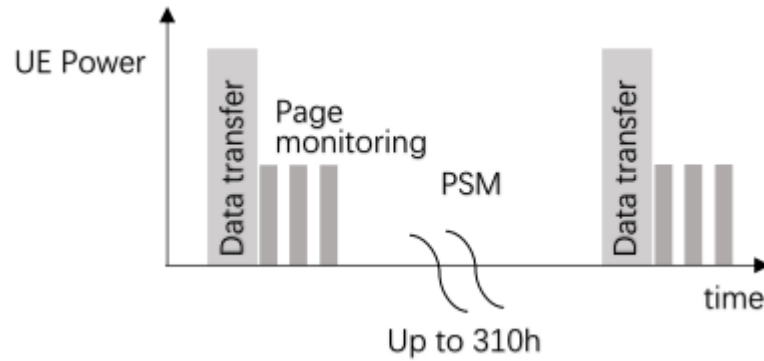


Figure 3.5 PSM scheme.

Extended discontinuous reception: eDRx is similar to DRx, which has idle and connected states (see Figure 3.6). However, eDRx supports longer period of paging monitoring for achieve power saving purposes. In addition, the conventional 2.56 s paging interval would result in severe power consumption for IoT devices, while downlink transmits data infrequently. Through the coordination of the core network and the terminal, the devices can skip most of the paging monitoring, and stay up to 2.91 h in disconnection state.

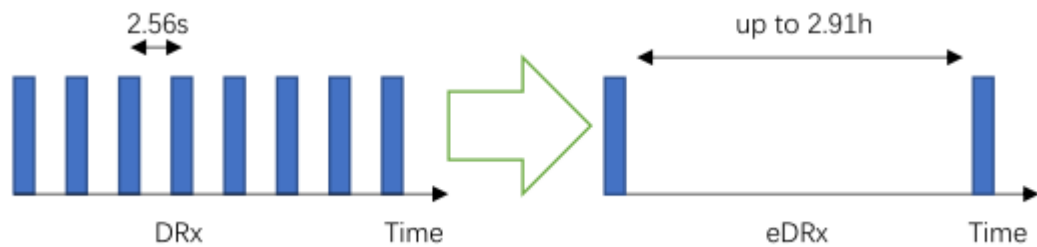


Figure 3.6 eDRx scheme.

From the above analysis, whether it is PSM or eDRx, it can be regarded as extending sleep duration to reduce power consumption, which actually sacrifices the real-time requirement [22]. In comparison, eDRx saves less power, but it has better real-time performance. This means that we need both PSM and eDRx scheme, they can be used to adapt to different scenarios, such as eDRX may be more suitable for object tracking, and PSM is more suitable for smart metering and environmental monitoring.

3.3.3 Reduced complexity

For the sake of mass-scale deployments, competing against existing IoT technologies such as Sigfox, LoRa, ZigBee, etc., NB-IoT scheme needs to reduce costs to facilitate market promotion. 3GPP effectively reduces the cost of NB-IoT communication modules to \$5 by simplifying the duplex model, the physical layer and the protocol stack, etc. [33]

Duplex mode: due to less-frequent data transmission, NB-IoT devices can simplify the F-FDD (full frequency division duplex) to H-FDD (half frequency division duplex), where

uplink and downlink transmissions are carried out on different carrier frequency bands but not at the same time (see Figure 3.7). This is similar to the basic GSM duplexing scheme. In this case, transceiver structure is simplified, and the cost of the duplexer is saved. Although NB-IoT has networking problems with TD-LTE, it can utilize GSM as an alternative method.

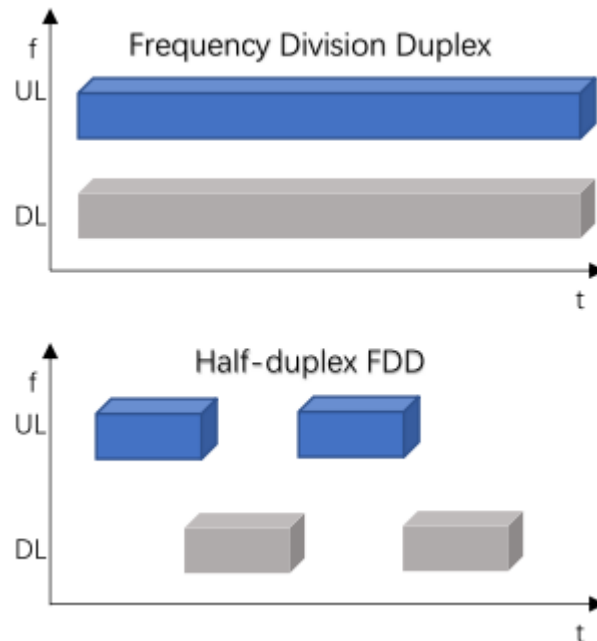


Figure 3.7 Frequency division duplex

Physical layer: the chip cost can be reduced through narrow bandwidth, low data rate and simplified channel in physical layer. NB-IoT terminal's working bandwidth is only 1 PRB (180 kHz) of conventional LTE. Narrow bandwidth helps it without complex equalization algorithms. Compared with LTE, the channel and physical layer process complexity is reduced by the narrow bandwidth also indirectly, such as PHICH (Physical Hybrid ARQ Indicator Channel), PCFICH (Physical Control Format Indicator Channel) and PUCCH (Physical Uplink Control Channel) are removed. In addition, NB-IoT only support a QPSK and BPSK modulations, which means ensured reliability but reduced data rates. [23]

Hardware simplification: Figure 3.8 illustrates the general NB-IoT devices hardware structure. We can see that the antenna model has changed from the original 1Tx/2Rx to the 1Tx/1Rx configuration. The complexity of the antenna, including antenna algorithms, will be effectively reduced. Moreover, low sampling rate and data rate can make cache/Flash RAM requirements reduced; low power consumption means that a simple and small PA (power amplifier) is enough, simplifying the RF design. Furthermore, NB-IoT devices remove the IP multimedia subsystem (IMS) stack directly, which means that it will not support the voice service.

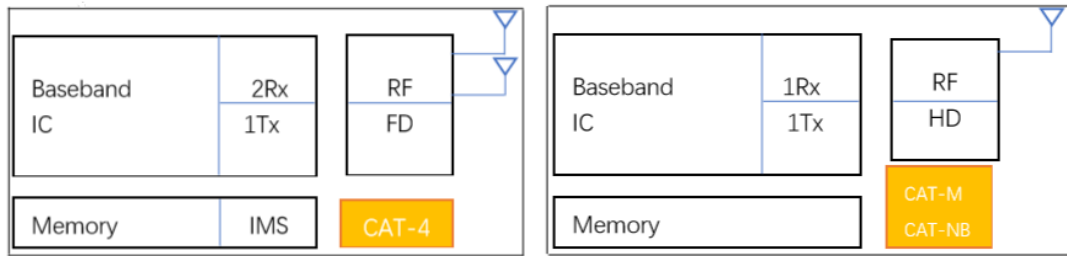


Figure 3.8 Popular CAT-4 (e.g. iPhone 6) and NB-IoT device hardware comparison.

3.3.4 Massive connectivity

NB-IoT aims to support a large number of low-throughput devices, i.e., a massive of connectivity. Each cell-site reaches 50K connections, which means that in the same base station, NB-IoT can provide 50~100 times more access than the existing wireless technologies. Next, we will introduce the 50K cell model, how to implement it and existing problems. [19][24]

The 50K NB-IoT user density is based on two hypotheses, one assuming that the number of NB-IoT devices in each family is 40, and the other is the density of the families in London. This is summarized in Table 3.3. [24]

Table 3.3 Device density assumption per cell [24]

Case	Household Density per Sq km	Inter-site Distance (ISD) (m)	Number of devices within a household	Number of devices within a cell site sector
Urban	1517	1732	40	52547

The 50K per cell-site goal benefits from traffic model and small uplink scheduling granularity. On one hand, NB-IoT is insensitive to latency, which enables more user access and user context. This allows around 50K terminals in a cell at the same time, while a large number of terminals stay in the sleep state, and the context information is maintained by the base station and core network. Once a device has data to send, it can quickly switch into the activated state. On the other hand, 2G/3G/4G systems have a large scheduling granularity, but due to the narrow bandwidth of NB-IoT, the granularity is smaller. The smaller the bandwidth, the smaller the uplink scheduling granularity. Single-tone NB-IoT uplink transmission has two alternative bandwidth, 3.75 kHz and 15 kHz. In the same resource situation, the utilization of resources will increase.

Massive connection capability requires independent access congestion control and optimization of the core network. NB-IoT can coexist with the current LTE and GSM. When NB-IoT is deployed in the 900 MHz LTE band, there is a case of NB-IoT and LTE common control, common BBU (baseband unit), etc. Because the typical number of users per cell of LTE is 400, undoubtedly, there is a need to design an independent access and

congestion control algorithm for NB-IoT. Moreover, even if the terminals go into the PSM sleeping state, the core network still needs to hold all the user's context data. Therefore, the massive permanent online users create new optimization requirements for the core network, regarding user context management, subscription, or the allocation of IP addresses. Compared to 4G, NB-IoT core network business suffers a strong burst, may be the user devices of a business service concentrated transmit and receive data at the same time, for example, smart metering services need to upload the user data in specific time of the month. This puts forward new requirements on core network equipment capacity and overload control.

3.4 NB-IoT numerology

3.4.1 Deployment modes

According to the NB-IoT PRB localization, three different operation modes can be defined: in-band, guard band, stand-alone [3][19]. From Figure 3.9, we can see that NB-IoT system can either occupy 1 PRB in LTE resources in the in-band option or exploit the unused guard band of LTE as transmission resource in the guard band option. In case of stand-alone, NB-IoT occupies a reframed GSM carrier. This model is also called EC-GSM-IoT.

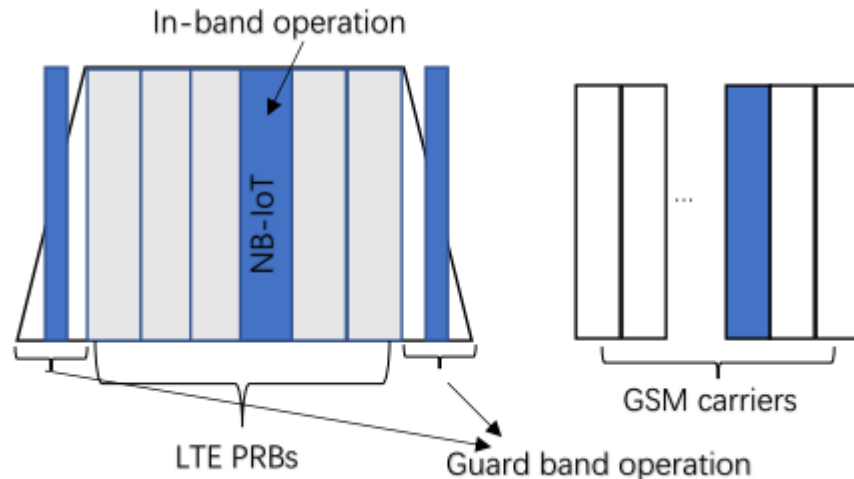


Figure 3.9 NB-IoT deployment options

We can summarize the different features of the three deployment modes as [25]:

- Spectrum: Need to consider coexistence with LTE system for in-band and guard-band operation regarding, e.g., interference avoidance, RF specifications. Stand-alone mode has independent spectrum.
- Base-station power: Stand-alone mode adopts a high downlink power, up to 20 W, while guard-band and in-band operation rely on LTE power without independent power control.

- Coverage: Stand-alone has a slightly larger coverage range, PBCH can reach 167.3 dB with 3 dB margin; coverage is slightly smaller with a limited PBCH of 161.1 dB in in-band and guard-band operation mode.
- Peak data rate: in general, Guard-band=In-band<Stand-alone.
- Latency: All meet the requirements, Stand-alone< Guard band<In-band.
- Current state: Stand-alone deployed by Vodafone in countries without LTE. Only Korea Telecom considers testing and validation Guard-band operation. Most LTE FDD operators have adopted the in-band operation scheme.

3.4.2 Frame structure

For communication systems, the physical layer frame structure is one of the underlying designs that determines basic principle of resource scheduling. The physical layer frame structure includes the frequency domain structure and the time domain structure.

Downlink

According to the system requirements of NB-IoT, the downlink radio frequency receiving bandwidth of the terminal is 180 kHz. Because of downlink 15kHz subcarrier spacing, NB-IoT keeps the original LTE design of downlink multiple access, frame structure and physical resource unit. [25]

In frequency domain, NB-IoT contains 12 available subcarriers with 15 kHz subcarrier spacing, which is illustrated in Figure 3.10.

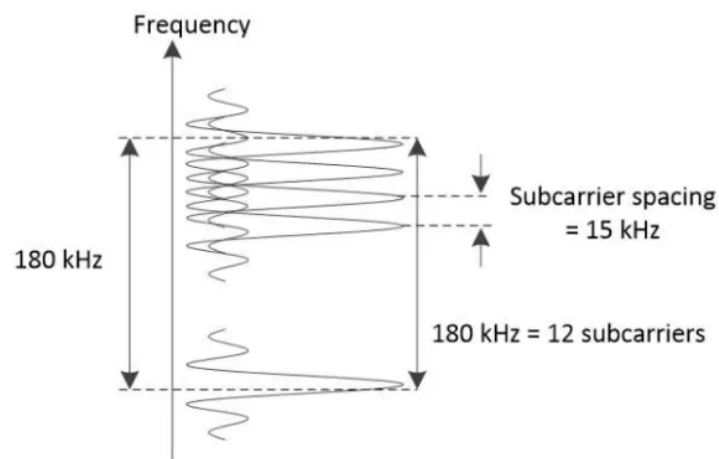


Figure 3.10 Frequency domain specifics

In time domain, NB-IoT has a slot length of 0.5 ms, and there are 7 symbols in each slot (see Figure 2.2 (a)). The basic scheduling unit is a subframe, two slots constitute a subframe, each radio frame includes 10 subframes. Hyper frame, new defined frame structure, contains 1024×1024 radio frames (up to 3h). In order to further save power, eDRx extends the paging cycle, and the terminal meets the goal of saving power by less paging messages. [25]

Uplink

In frequency domain, NB-IoT occupation bandwidth is 180 kHz. The uplink supports multitone and single-tone transmission and uses $\pi/2$ BPSK or $\pi/4$ QPSK modulation to lower the PAPR. Multitone transmission utilizes SC-FDMA based on 15 kHz subcarrier spacing, while single-tone scheme enables 3.75 kHz and 15 kHz bandwidth two alternative subcarrier spacings. Single-tone means that only one subcarrier is carrying each user's data, which is like a single OFDM subcarrier modulation. The 3.75 kHz in-band case will inherently interfere with LTE system and, therefore, effectively power control is important to keep the interference to neighbor LTE PRB at an acceptable level. On the other hand, all the 15 kHz cases maintain orthogonality, and they can coexist with the LTE system. However, the NB-IoT signal needs to be well-synchronized to the LTE network to reach this. [3][25]

15 kHz subcarrier spacing: maximum support for 12 subcarriers, and the frame structure will be consistent with the LTE. We can schedule one or multiple subcarriers to transmission.

3.75 kHz subcarrier spacing: the newly defined frame structure supports the maximum of 48 subcarriers within the 180 kHz band. It brings two advantages: On the one hand, compared to 15 kHz, 3.75 kHz will have considerably higher PSD, which will translate into coverage. On the other hand, within the limited 180 kHz spectrum resource, the scheduling resource is extended from the original 12 subcarriers to 48 subcarriers, which can provide more flexible scheduling (see Figure 3.11).

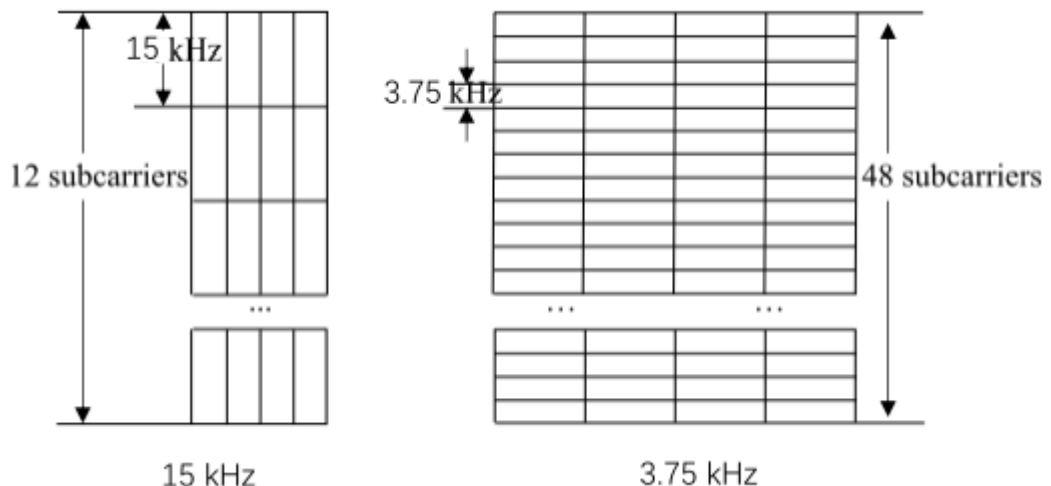


Figure 3.11 Frame structure for 3.75 kHz and 15 kHz subcarrier spacing cases

In time domain, the basic time resource unit of uplink is slot. For the 15 kHz subcarrier spacing, 1 slot=0.5 ms, which is consistent with LTE. But for 3.75 kHz subcarrier spacing, 1 slot=2 ms.

4. SYSTEM MODEL

4.1 Overview

This system model is based on NB-IoT in-band operation, and generally basic system model is illustrated in Figure 4.1. The uplink model contains two sub-band signals, which utilize SC-FDMA for NB-IoT and OFDM for LTE. We simulate LTE by OFDM, because most of the 5G uplink users (especially the ones with a good channel and high data rate) will use OFDM also in uplink. SC-FDMA will be used only for extreme pathloss (cell edge) cases. So OFDM model is quite relevant and more straightforward. Our main target is to verify whether the filtered sub-band method can support asynchronous uplink NB-IoT transmission next to OFDM subcarriers in adjacent LTE resource blocks.

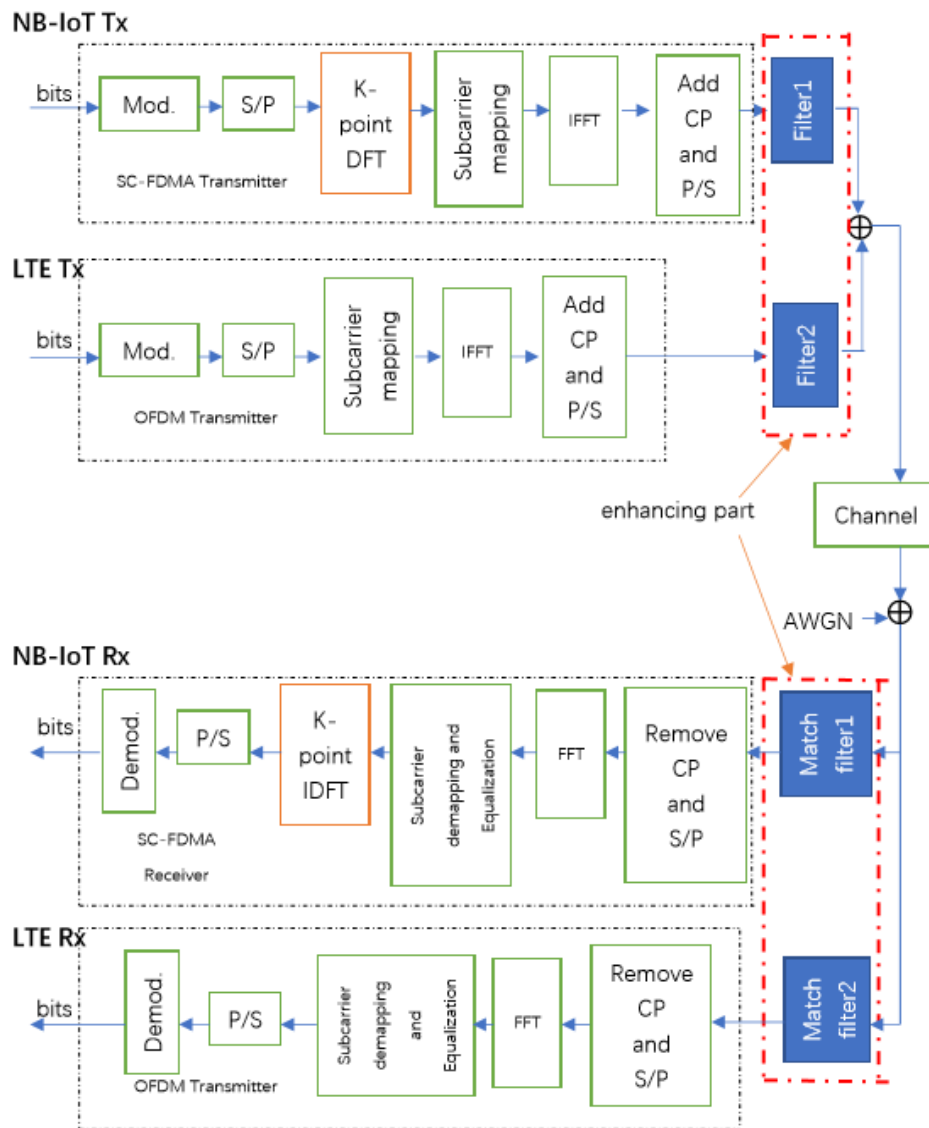


Figure 4.1 Basic in-band system block diagram

Table 4.1 summarizes the system configuration. The simulation bandwidth is 1.4 MHz, which contains 5 PRBs of LTE signal and 1 PRB for NB-IoT. Both NB-IoT and LTE have the same subcarrier spacing. In Release 13, NB-IoT in-band operation is based on the SC-FDMA waveform, but SC-FDMA waveform has high out-of-band emission, similar to OFDM of the cellular uplink, and the signals will interfere each other, unless they are perfectly synchronized. To increase the spectrum concentration, we can use the filtered OFDM waveform, proposed by Huawei, to suppress the spectrum leakage.

For the sake of simplification, we put the NB-IoT spectrum centered at DC (see Figure 4.2 (a)). In this way, we can design a low pass filter for the NB-IoT signal, and use the same filter as matched filter on the receiver side. In practical implementation, NB-IoT PRB should schedule exactly one PRB, which cannot be DC-centered (see Figure 4.2 (b)). In this case, we can shift the filter of NB-IoT to be centered at the target PRB by multiplying its impulse response with the complex exponential $e^{j*2*\pi*f*n/N_IFFT}$, where f is the center frequency of the target PRB.

Table 4.1 System parameters

General parameters	Value
System bandwidth	1.4 MHz
Number of PRBs	6
FFT size	128
Subcarrier spacing	15 KHz
Total CP length in a slot	0.5T
Subframe length	1 ms
Sampling rate	1.92 MHz
Symbols/Subframe	14

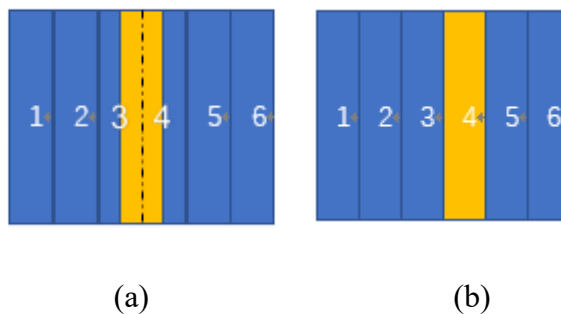


Figure 4.2 The blue and yellow color indicates the LTE and NB-IoT respectively, each strip has 12 subcarriers. (a) The NB-IoT PRB centered in LTE band with half of an LTE PRB on both sides. (b) In practical, we allocate NB-IoT to a PRB with index 1 to 6.

In one slot, which has $1.92\text{MHz} \times 0.5\text{ms} = 960$ samples, we need to add the total CP length of $960 - 7 \times 128 = 64$. Thus, the CP length is 10 for first OFDM symbol and 9 for the other 6 symbols. We perform the CP adding along with the parallel to series (P/S) process, which is illustrated in Figure 4.3.

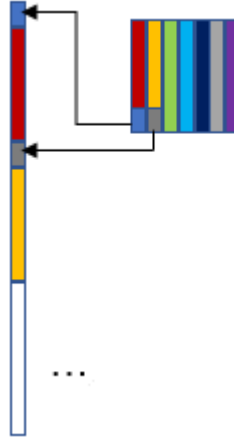


Figure 4.3 CP adding and P/S process: 1. Take the last ten samples of first column and put the ten samples in the first ten samples place. 2. Perform the same process with nine samples for columns two to seven. 3. Repeating steps 1 and 2 for each slot.

4.2 System aspects

Table 4.2 illustrates the specific configurations of NB-IoT and LTE signals. We can see that the NB-IoT signal utilizes $\pi/2$ -BPSK modulation with SC-FDMA. Compared with BPSK, $\pi/2$ -BPSK modulation has lower peak to average power ratio (PAPR), which is an additional method to minimize PAPR.

Table 4.2 NB-IoT and LTE configuration

Type	Modulation	Active Scs	Waveform	Filter type	Equalizer	Channel
NB-IoT	$\pi/2$ -BPSK	10 or 12	SC-FDMA	Low pass	Zero-forcing	AWGN
LTE	QPSK (4QAM), 64QAM	60	OFDM	High pass	Zero-forcing	AWGN

4.2.1 $\pi/2$ -BPSK

In R1-1613597, $k\pi$ BPSK (e.g., 0.5π BPSK or 0.25π QPSK) was proposed as an additional PAPR minimization method.

At first, let's have an in-depth consideration of the $\pi/2$ -BPSK modulation scheme. You may think that it just rotates the phase by $\pi/2$ from the normal BPSK constellation, however, the $\pi/2$ -BPSK scheme is a mix of normal and $\pi/2$ phase rotated BPSK constellation.

More specifically, we define the transmission sequence (size [1920, 1] in our case) where odd index and even index constellations are normal BPSK and $\pi/2$ phase shift BPSK, respectively [26][27][28]. Figure 4.4 shows a transmission sequence with $\pi/2$ -BPSK modulation. The signal generation could utilize the Matlab `diag` function instead of for loop, which can improve the code efficiency.

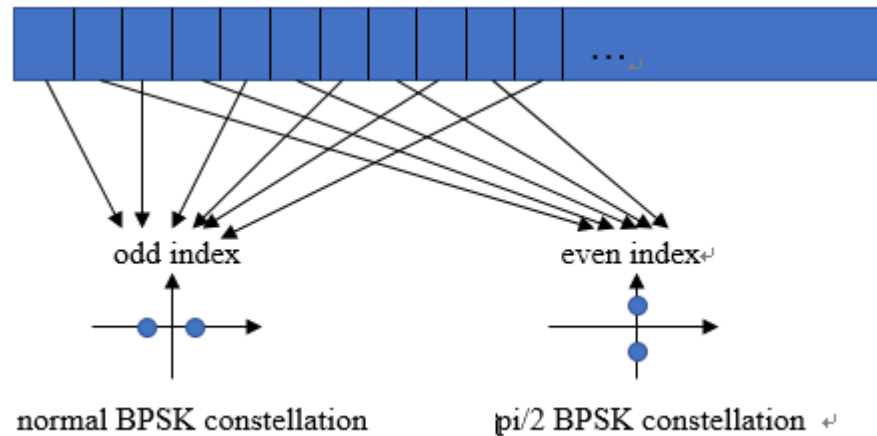


Figure 4.4 $\pi/2$ -BPSK modulation scheme

4.2.2 Transmission end signals and AWGN channel

NB-IoT signal is based on the SC-FDMA scheme, which needs a scaling factor $\sqrt{1/N_{sc}}$ to keep the signal power level same as OFDM (see Figure 4.5). This is caused by the DFT (FFT) process before the IFFT operation.

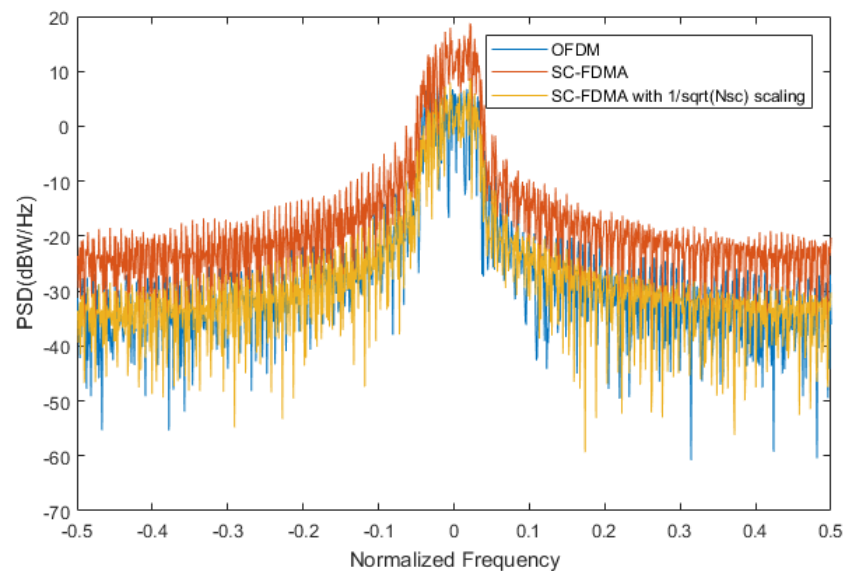


Figure 4.5 Scaling factor effect on SC-FDMA spectrum. N_{sc} is the number of subcarriers

After generating the transmission end signal (see Figure 4.6), we add the additive white Gaussian noise (AWGN) to the system. AWGN can help us to analyze the noise immunity of the system. The reason is:

1. Gaussian white noise can be expressed by a specific mathematical expression, easy to derive analysis and implementation.
2. Gaussian white noise does reflect the additive noise in the real channel, and simulates the random process of the nature.

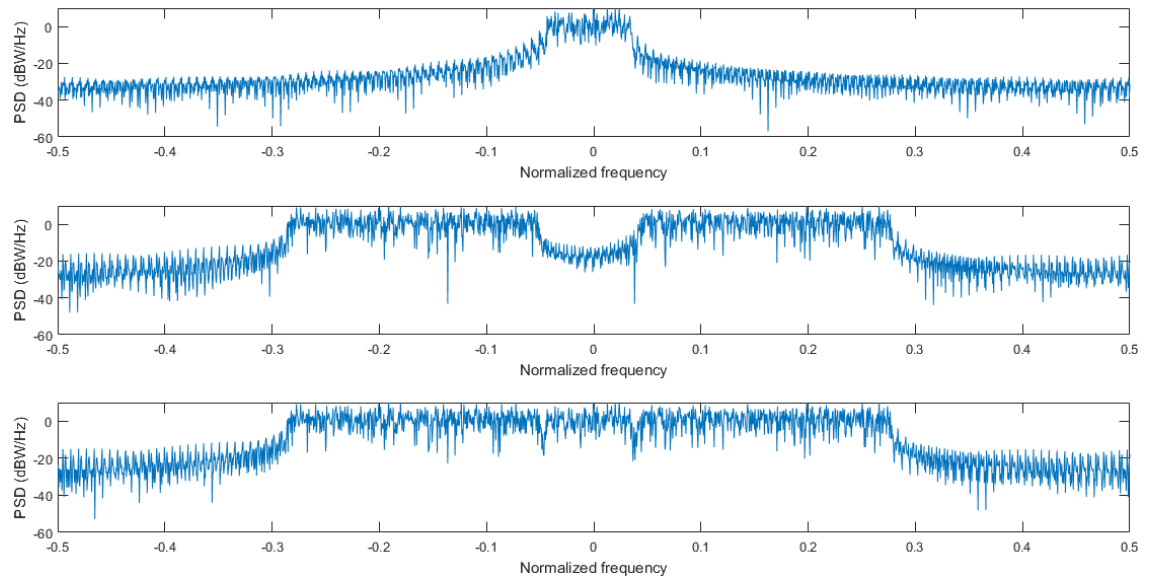


Figure 4.6 Transmission end signal PSDs with AWGN. The NB-IoT signal utilizes 10 active subcarriers and two guard tones, LTE signal has 60 active subcarriers. Upper: 1 PRB NB-IoT UEs data, DC-centered. Middle: 5 PRBs LTE UEs data with 1 PRB reserved for NB-IoT. Lower: Joint PSD of the two sub-bands signals.

Before we add the AWGN, let's have an in-depth discussion about the noise scaling factor, since it is a basic and essential part to get correct bit error ratio (BER) metrics in Monte Carlo simulations. At the transmission end, signals are transmitted in the form of symbols. Noise is easily generated based on E_s/N_0 (energy per symbol to noise power spectral density) as the following equation:

$$\text{required noise} = 10^{\frac{E_s}{N_0} - 10} \times \text{noise} \quad (4.1)$$

Here 'noise' means a zero-mean unit-variance-noise sequence and the received signal is assumed to have unit variance. The connection between E_s (energy per symbols) and E_b (energy per bit) can be written as:

$$E_s = G \cdot E_b \quad (4.2)$$

where G is the number of bits per symbol. The practical BER performance metric is based on E_b/N_0 (energy per bit to noise power spectral density ratio), thus, we need to find the relationship between E_b/N_0 and S/\mathcal{N} (i.e. SNR), where S is the signal variance and \mathcal{N} is the noise variance. This is caused by the time domain and frequency domain overheads of the transmission scheme. In the time domain, CPs are added to the transmitted sequence. On the other hand, some subcarriers, without carrying data bits, are served as guard tones in the frequency domain. [29][30]

Since the added CP does not carry any additional information, the transmitted symbol contains both useful and overhead energy [31]. The bit energy represents the energy only contained in useful symbol period. Figure 4.7 shows the CP addition process for one symbol. We can see that symbol energy is spread over time $T_g + T_b$, which length is $N_{cp} + N$ samples, where N is the IFFT size. Moreover, the bits energy is spread over the time T_b , which contains N bits. Thus, for a N_{act} active subcarriers OFDM or SC-FDMA signal, the signal variance can be given by:

$$S = N_{act} \cdot \frac{E_s}{T_g + T_b} = N_{act} \cdot \frac{E_s}{T_b} \cdot \frac{T_b}{T_g + T_b} \quad (4.3)$$

equivalent bits ratio is easy to deploy:

$$S = N_{act} \cdot \frac{E_s}{N} \cdot \frac{N}{N_{cp} + N}, \quad (4.4)$$

and the noise variance \mathcal{N} :

$$\mathcal{N} = N_0 \cdot W = \frac{N_0}{T_b} = \frac{N_0}{N}, \quad (4.5)$$

where W is the total bandwidth.

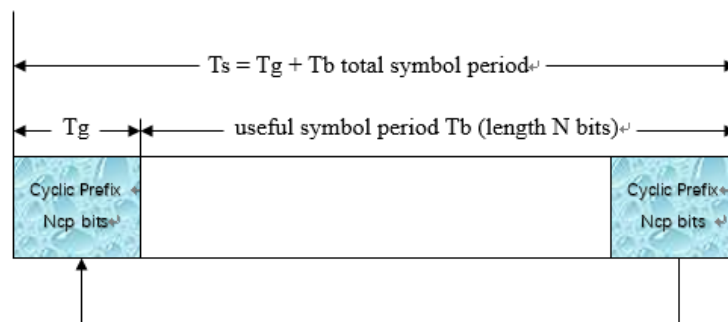


Figure 4.7 Time domain overhead

Thus,

$$S/\mathcal{N} = \frac{E_s}{N_0} \cdot N_{act} \cdot \frac{N}{N_{cp} + N}$$

$$= G \cdot \frac{E_b}{N_0} \cdot N_{act} \cdot \frac{N}{N_{cp}+N}. \quad (4.6)$$

The simulation noise scaling factor K can be calculated by:

$$K = \sqrt{S/\mathcal{N} \cdot 10^{-SNR_{target}/10}}, \quad (4.7)$$

for the sake of generating the required SNR, we assume the noise bandwidth is equal to the signal bandwidth.

From Figure 4.8, we can observe that the simulated result accords with the theoretical BPSK bit error rate, the theoretical BER model of BPSK is given by:

$$P_{b,BPSK} = \frac{1}{2} \operatorname{erfc}\left(\sqrt{\frac{E_b}{N_0}}\right). \quad (4.8)$$

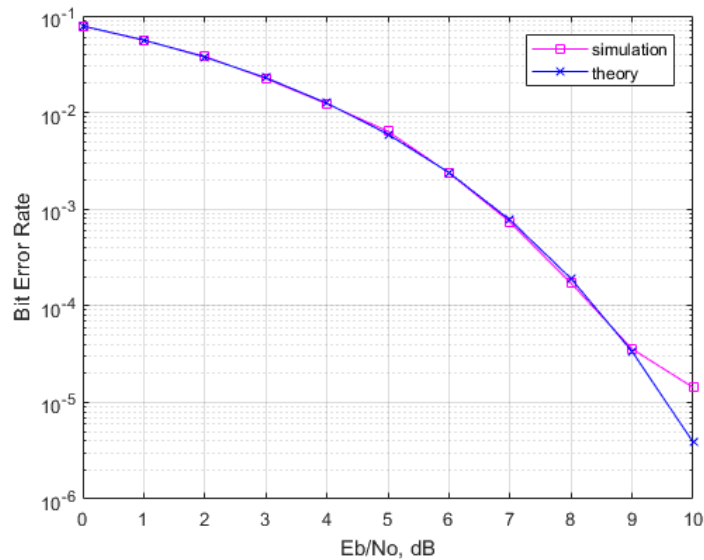


Figure 4.8 BER curve comparison based on BPSK

4.3 Implementation of Filtered OFDM

As we mentioned before, Figure 4.1 presents a NB-IoT system block diagram for in-band operation, which is a typical OFDM/SC-FDMA system. In most cases, the LTE signal has higher power level in the base-station receiver than the NB-IoT signal, in order to support higher-order modulation. Then the NB-IoT signal performance will be limited by the higher OOB of the LTE transmission. This is critical in asynchronous transmission, because strict time-frequency alignment of different uplink users' signals at the base-station receiver is required to maintain orthogonality. Thus, we use filtered OFDM waveform, a promising 5G waveform candidate, reducing potential inter-carrier interference due to asynchronous operation or mixed numerologies [6][7].

To simply analysis, we consider one sub-band Tx part in Figure 4.1. The transmission signal can be written by:

$$x(n) = \left[\sum_{l=0}^{L-1} s_l(n - l(N + N_{cp})) \right] * f(n), \quad (4.9)$$

with

$$s_l(n) = \sum_{k=k'}^{k'+K-1} d_{l,k} e^{\frac{j2\pi kn}{N}}, \quad -N_{cp} \leq n \leq N,$$

where N_{cp} is the CP length, $d_{l,k}$ denotes the data symbol of k th subcarrier and l th OFDM symbol, and $f(n)$ means the corresponding sub-band filter impulse response. In case of SC-FDMA, $d_{l,k}$ are the values obtained from the DFT.

Filter design

The filter design is a key element of the f-OFDM system. In this thesis work, we utilize the following filter types: windowing method, root-raised-cosine (RRC), and equiripple design, which were mentioned in Section 2.3.2.

Windowed sinc filters: We consider applying Hann window and Hamming window $w(n)$ to approximate the ideal low-pass filter $p_B(n)$, i.e.

$$f_B(n) \triangleq p_B(n) \cdot w(n), \quad (4.10)$$

where $p_B(n)$ is ideal low-pass filter $p_B(n) = \frac{w_c \sin(w_c n)}{\pi w_c n}$. The specific expression for Hann window is:

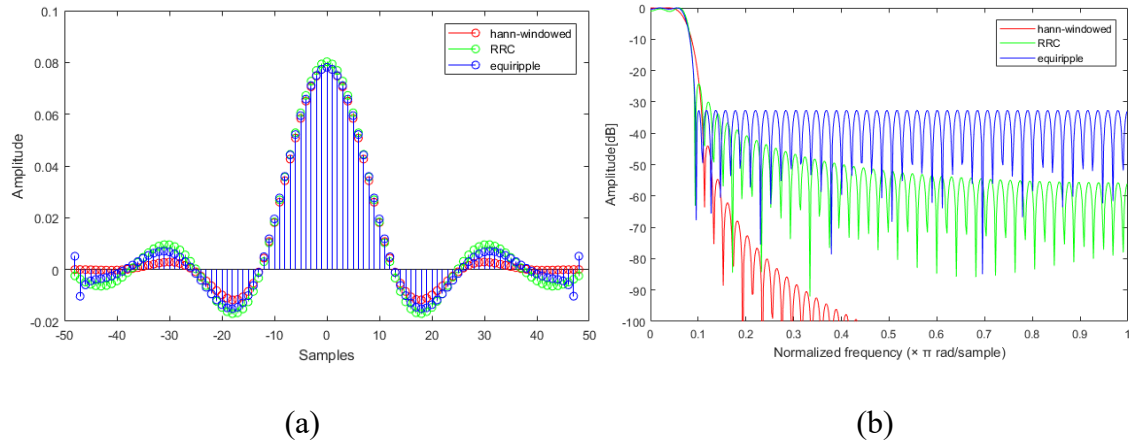
$$w(n) = 0.5 \left(1 + \cos \frac{2\pi n}{M} \right), \quad (4.11)$$

where, M is filter length. In our case, we need a fairly narrow transition bandwidth, in order to combine NB-IoT and LTE PRB's without too much guard-band. For the stopband attenuation, 20 dB was found to be sufficient. Owing to the centered model of the NB-IoT PRB, we simply utilize the low-pass filter for NB-IoT and high-pass filter for LTE. [32]

Figure 4.9 presents an example of a NB-IoT low-pass filter based on the configuration of Table 4.3. Although the Hann windowed sinc filter has a quickly decaying impulse response, its stopband attenuation is the smallest (see Table 4.4). Actually, the Hann windowed filter needs at least four transition band subcarriers. Thus, in the following experiments, we test the RRC and equiripple filters only.

Table 4.3 Filter configuration for NB-IoT

Parameters	Value
Subcarrier spacing (kHz)	15
NB-IoT bandwidth (kHz)	180
Sampling frequency (MHz)	1.92
Transition band subcarriers	2
Passband edge (kHz)	4*15
Stopband edge (kHz)	6*15

**Figure 4.9** (a) Impulse responses of different filters, (b) Frequency responses of different filters**Table 4.4** Different filters features based on the configuration of **Table 4.3**

Case	Passband ripple (dB)	Stopband attenuation (dB)
Hann-windowed	1.3253	14
RRC	1.1381	24
Equiripple	0.4152	25

After designing a sub-band filter with good characteristics, then we need considering sub-band signal filtering. The implementation process can be carried out in the time domain, or in the frequency domain. Time domain filtering is achieved by linear convolution. Assuming that the filter impulse response is $f'(n)$ with length $M + 1$, then the filtering operation can be expressed by:

$$y(n) = x(n) * f'(n) = \sum_{m=0}^M x(n - m) f'(m). \quad (4.12)$$

In the filtered OFDM system, a longer filter could be used to obtain a lower out-of-band spectral leakage, but it could destroy the time domain orthogonality between successive OFDM symbols. At the same time, to ensure the continuity of the sub-band signal filtering, we need to remove the delay caused by the convolution process. In this way, the continuity of the filtering process can be guaranteed, and the specific implementation process is shown in Figure 4.10.

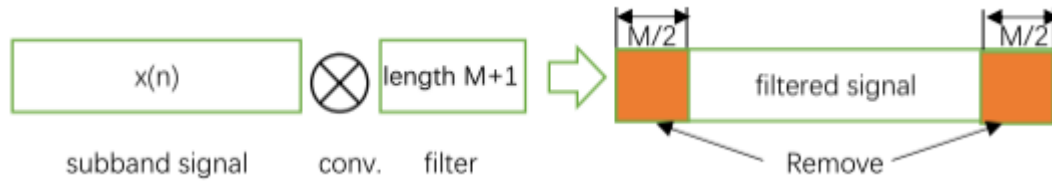


Figure 4.10 Time-domain filtering process assuming that the filter length $M + 1$ is odd.

Assuming the total length of the data is N , then the total number of complex multiplications of time-domain filtering is in the order of $N*M$. In f-OFDM, to control sub-band interference, the filter length M is usually relatively large, which causes a high computation complexity in the filtering operation. For the sake of time-domain filtering complexity, the filtering process can be realized in the frequency-domain with a significantly lower complexity.[34][35][36]

As for LTE band, when the NB-IoT PSD is significantly lower than that of LTE, NB-IoT performance will be affected. Therefore, the LTE band also needs to be filtered. Since we reserved one PRB wide DC-centered resource for NB-IoT UEs (see Figure 4.2), we can deploy LTE a high pass filter with stopband and transition bands within the NB-IoT PRB, minimizing the impact on the original spectrum of LTE. Due to the transition band localization, we can design the LTE filter as the complementary highpass filter of lowpass filter of NB-IoT. Assuming that symmetric, linear-phase FIR filters of length $M + 1$ (odd) are used, this solution can be written as:

$$H_{HP}(z) = z^{-\frac{M}{2}} - H_{LP}(z). \quad (4.13)$$

4.3.1 Symmetrical filtering process

To effectively filter the subcarriers, we need to consider the exact location of the transition band edges. For example, the following figure shows NB-IoT filtering process (LTE filtering process is similar), NB-IoT has 10 active subcarriers without DC, and has one guard tone on both sides. Assume we select filter configuration with passband edge is four, and stopband edge is six (see the red lines contour). To perform the symmetrical filter process, we shift the signal spectrum to the right side with 0.5 subcarrier spacing before filtering it. In Figure 4.11, the black line represents subcarriers and short blue line on the outside of the black line is guard tone.

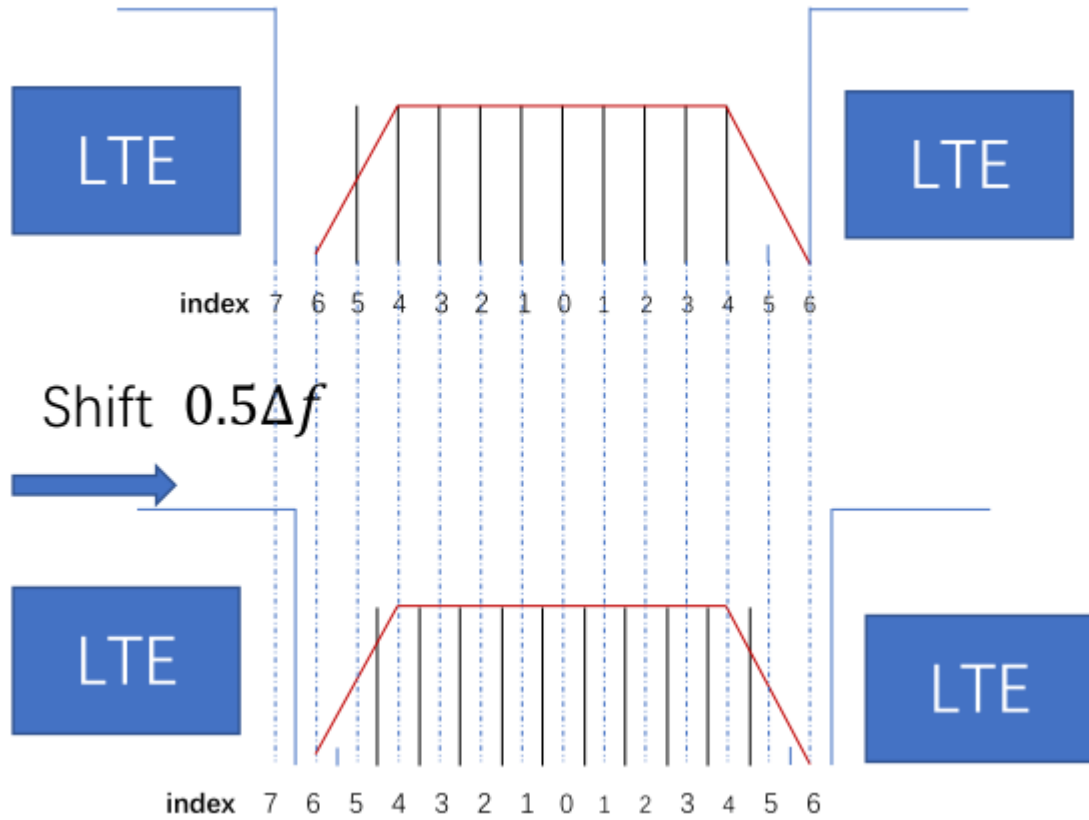


Figure 4.11 Symmetric lowpass filter model for NB-IoT

After the filtering process, the filtered signal needs to be shifted back correspondingly. The overall process is given by:

$$y(n) = [(x(n) \cdot e^{j2\pi(0.5\Delta f)n}) * h(n)] \cdot e^{j2\pi(-0.5\Delta f)n} \quad (4.14)$$

4.4 PAPR

OFDM signal can be seen as a sum many subcarrier tones with independent amplitude and phase factors. This cause a much higher peak value in time domain than that in a single-carrier system. Undeniably, the high PAPR characteristic is one of the most unfavorable aspects in OFDM system, which results the OFDM system suffering from signal-to-quantization noise ratio (SQNR) decrease both in analog-digital converter (ADC) and digital-analog converter (DAC). Moreover, nonlinear distortion is most likely to occur in the transmitter power amplifier (PA) with high PAPR waveforms, so this problem will bring great challenges to the PA design, especially for the mobile terminal. [18]

PAPR is maximum squared magnitude value of a baseband signal divided by average value of this signal (also known as mean-squared value), i.e.,

$$\gamma_c = \frac{\max_{0 \leq t \leq T} |s(t)|^2}{E\{|s(t)|^2\}} = \frac{\max\{s(t)s^*(t)\}}{E\{s(t)s^*(t)\}}, \quad (4.15)$$

where T is the symbol interval, and $()^*$ represent a complex conjugate operation. The real part and image part probability distribution functions (PDFs) of OFDM signal follows Gaussian distribution, which makes OFDM signal waveform similar to Gaussian noise. As an example, Figure 4.12 shows the PDF of a 12 subcarriers OFDM signal, using BPSK modulation.

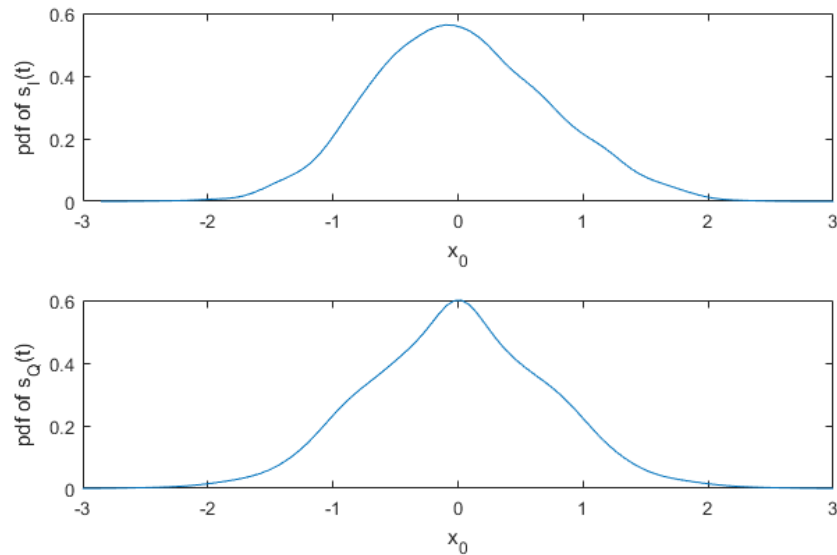


Figure 4.12 PDF of the real part (upper) and imaginary part (lower) of an OFDM signal.

In practice, we utilize the complementary cumulative distribution function (CCDF) to evaluate the PAPR characteristics of a signal. Firstly, the average power level is supposed to be normalized to 1. Secondly, we define that horizontal and vertical axis are power level [dB] and the corresponding CCDF, respectively. The PAPR curve (see Figure 4.13) gives the probability (read from CCDF vertical axis) of the power level reaching or exceeding from the value on the horizontal axis.

In the literature, there are numerous methods for mitigating the high PAPR of OFDM signals, but these methods usually increase the complexity of system. In this thesis, the PAPR is mitigated by the $\pi/2$ -BPSK SC-FDMA method. Figure 4.13 presents a PAPR comparison between BPSK SC-FDMA and $\pi/2$ -BPSK SC-FDMA. This simulation case is based on 12 subcarriers, 14 symbols, and 128 points IFFT. As it can be seen in Figure 4.13, the peak power level of those signals reaches or exceeds 4.9 dB and 6.5 dB respectively. It is obvious that the $\pi/2$ -BPSK SC-FDMA scheme brings approximately 1.6 dB lower peak power level.

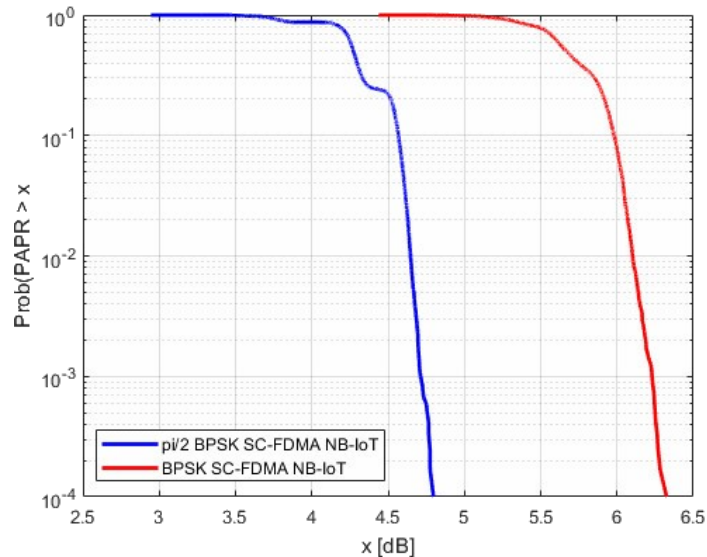


Figure 4.13 PAPR comparison between $\pi/2$ BPSK and BPSK based SC-FDMA signals.

4.5 Matched filtering

Since the in-band deployment model is generated by combination of NB-IoT and LTE sub-bands, the receiver signal processing is divided into two sub-band branches after the corresponding sub-band matched filtering process. The received signal at base-station can be written as:

$$y(n) = \sum_{i=1}^D s_i(n - n_i) * h_i(n) + z(n), \quad (4.16)$$

where n_i denotes the delay between UE_i and base-station, $h_i(n)$ is channel impulse response between UE_i and base-station, $z(n)$ is the additive Gaussian noise, and D is the number of uplink users. The matched filter filtered sub-band signal can express as:

$$y'_i(n) = y(n) * f_i^*(-n), \quad (4.17)$$

where $f_i^*(-n)$ is the i sub-band filter in receiver side, which is matched to the transmitter filter.

There are two main benefits of sub-band matched filtering. One is that the matched filter can filter out interference from the other sub-band signals while keeping the target sub-band signal. For example, the NB-IoT data locates at low-frequency part in our system model, and we use the same low-pass filter on the receiver side to filter out the high-frequency components due to LTE. On the other hand, the signal-to-noise ratio of the received signal can be maximized by correctly performing the signal detection. The receiver processing is done separately for each user's signal. In this way, the receiver complexity is related to the number of users.

4.6 Equalizer

The channel transfer function is a random process due to the existence of frequency selective fading, Doppler shift, etc. In order to address this problem and compensate the filtering effect, we first need to estimate the channel effect on each active subcarrier. The channel estimation is commonly based on pilots, which are specific transmitted data symbols known by the receiver.

Channel model

The multipath channel model can be written as:

$$h(t) = \sum_{c=1}^{L_p} h_c(t)\delta(t - \tau_c(t)). \quad (4.18)$$

Here, we can assume that the multipath gains $h_c(t)$ and multipath delays $\tau_c(t)$ are constant in a OFDM symbol time interval. For the simulation experiments reported later, we select the ITU-R Vehicular-A channel model, the parameters of which are presented in Table 4.5. In our system model, the cyclic prefix length is $4.69 \times 10^{-6}s$, which is greater than that of the maximum multipath delay ($2.51 \times 10^{-6}s$). Therefore, we can assume that there is no ISI between adjacent OFDM symbols. Then the OFDM system is equivalent to X_{N-1} parallel flat-fading transmission system, as shown in Figure 4.14.

The frequency domain channel response at the m th carrier frequency of the n th OFDM symbol can be expressed as:

$$H_{mn} = \sum_{c=1}^{L_p} h_c(n)\exp(j2\pi m \frac{\tau_c(n)}{T}). \quad (4.19)$$

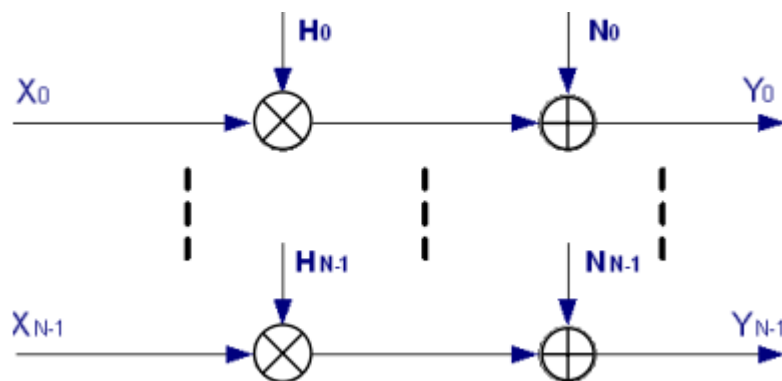


Figure 4.14 Equivalent model for frequency-selective multipath channel when the CP length exceeds the channel delay spread.

After CP removal and FFT processing on the receiver side, we can get the received signal of the m th carrier frequency of the n th OFDM symbol as:

$$Y_{mn} = H_{mn}X_{mn} + N_{mn}, \quad (4.20)$$

where N_{mn} is the AWGN at the FFT output.

Table 4.5 Veh-A channel model.

Type	Values
Path delays (s)	[0 310 710 1090 1730 2510]*1e-9
Path gains (dB)	[0 -1 -9 -10 -15 -20]

Zero-forcing Equalization

Typically, the medium through which the OFDM signal passes from a transmitter to a receiver is viewed as a time-varying multipath channel. The channel estimation should be able to estimate the channel response of subcarriers at any time. The structure of the OFDM signal enables us to use the time-frequency two-dimensional estimation method. And the correlation of the wireless channel in the time-domain and the frequency-domain allows us to place pilots on a limited number of OFDM symbols and subcarriers. Here we do not consider using the guard interval for channel estimation. In an OFDM system, the general equalization method has two types: frequency-domain equalization and time-domain equalization. Frequency-domain equalization means equalizing the received signal after the FFT process in the receiver. On the contrary, time-domain equalization equalizes the receiver signal before the FFT process of receiver. Since the CP length is greater than the maximum channel delay spread, we select the frequency-domain equalization, which is used in practically all OFDM systems. [37]

The de-multiplex $Y(k)$ of received samples $y(n)$ is

$$Y(k) = DFT\{y(n)\} = \frac{1}{N} \sum_{n=0}^{N-1} y(n) e^{-\frac{j2\pi kn}{N}}, k = 0, 1, \dots, N-1 \quad (4.21)$$

$$= X(k)H(k) + W(k)$$

where $H(k)$ denotes a channel or a filter frequency response, $W(k)$ is AWGN noise. The frequency domain zero-forcing equalizer $C(k)$ is implemented in the de-multiplex data:

$$Y_{ZF}(k) = Y(k)C(k) \quad (4.22)$$

a) Equalization with AWGN channel

We calculate the corresponding filter frequency response $F(k)$, and use it to get the channel equalizer weights to minimize the filtering effect on active subcarriers. The zero-forcing equalizer is expressed as:

$$C(k) = 1/F(k) \quad (4.23)$$

In this case, we do not consider minimizing the effects of AWGN, but the results are acceptability and the implementation is straightforward.

b) Equalization with frequency-selective channel

On the receiver side, we calculate the pilots based equalization coefficients $\widehat{C}_p(k)$ for each active subcarrier, compensating the joint amplitude attenuation and phase rotation caused by channel transform function and the filters [38][39]. We generate BPSK training symbols on the transmitter side, packed with UEs data symbols and transmitted through the channel. Then, estimate the received pilot based equalization coefficients in simplified scenarios where the interference leakage effects are absent. The received pilots are obtained by $\{Y(k)\}$ and then the channel estimation can be written as

$$1/\widehat{C}_p(k) = \frac{Y_P(k)}{X_P(k)} + \frac{W(k)}{X_P(k)} \quad (4.24)$$

This is done in order to avoid working out channel estimation enhancements for the practical scenarios where the interference is present. The results are anyway closer to reality than those based on the common assumption of ideal channel knowledge.

4.7 Power level model

To avoid the near-far problem, we need to control the power levels of users at different distance from the base station. However, for uplink power control, a higher power level will increase the interference to each other. The target spectrum density (i.e., subcarrier power levels) depend on the modulation order and code rate, based on the required SNR for sufficient performance. This could be based on LTE specs, but to simplify things, we can just use the SNR required ideally for 1% uncoded BER for BPSK, QPSK and 64QAM (see Figure 4.15).

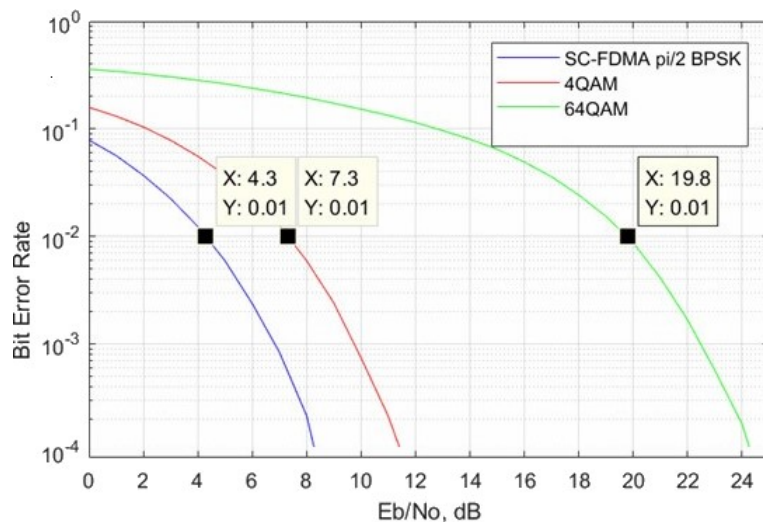


Figure 4.15 Ideal BER curves for BPSK, QPSK and 64QAM, and required SNRs for 1% uncoded BER.

We can see when the BER target is set at 0.01, the BPSK, QPSK and 64QAM optimal power levels corresponding to the SNRs of 4.3 dB, 7.3 dB, and 19.8 dB, respectively. In uplink transmission, base-station may experience significant variations from the optimum. Assuming ± 12 dB relative power variations, we can summarize the optimum and critical testing cases as follows:

Optimum power test cases:

- NB-IoT and LTE/QPSK at optimum level: $4.3-7.3=-3$ dB. Average power of NB-IoT subcarriers is 3 dB weaker than that of LTE.
- NB-IoT and LTE/64QAM at optimum level: $4.3-19.8=-15.5$ dB. Average power of NB-IoT subcarriers is 15.5 dB weaker than that of LTE.

Critical test cases:

1. NB-IoT

- NB-IoT 12 dB weaker than optimum with LTE/QPSK: $4.3-12-7.3=-15$ dB. Average power of NB-IoT subcarriers is 15 dB weaker than that of LTE.
- NB-IoT 12 dB weaker than optimum with LTE/64QAM: $4.3-12-19.8=-27.5$ dB. Average power of NB-IoT subcarriers is 27.5 dB weaker than that of LTE.

2. LTE

- NB-IoT 12 dB stronger than optimum with LTE/QPSK: $4.3+12-7.3=9$ dB. Average NB-IoT subcarrier is 9 dB stronger than LTE subcarrier.
- NB-IoT 12 dB stronger than optimum with LTE/64QAM: $4.3+12-19.8=-3.5$ dB. Average NB-IoT subcarrier is 3.5 dB weaker than LTE subcarrier.

Therefore, we can summarize testing cases in Table 4.6.

Table 4.6 The average subcarrier power scaling, K is the scaled signal average subcarrier power difference, $K = P_{avNB-IoT} - P_{avLTE}$.

Case	4QAM	64QAM
Optimum test K (dB)	-3	-15.5
NB-IoT critical test K (dB)	-15	-27.5
LTE critical test K (dB)	9	-3.5

5. RESULTS AND ANALYSIS

5.1 AWGN channel testing

We simulate the NB-IoT in-band mode performance under configurations defined by Table 4.1 and Table 4.2, assuming the worst CFO and TO between the two sub-bands, i.e., 0.5 subcarrier spacing and 0.5 symbol duration, respectively. In addition, suitable filters are selected from the following filter candidates: 1. Windowed sinc filter includes Hann window, Hamming window, Huawei proposed 0.6-powered raised cosine (0.6 RC) window [34][35], 2. Equiripple filter, 3. RRC. As we mentioned before, we put the NB-IoT PRB symmetrically around 0-frequency, and the filter transition bandwidth should be fairly narrow.

Therefore, we test all the filters with a reasonable configuration: length 97, passband edge 4×15 kHz, stopband edge 6×15 kHz. At first, let's have a look at the NB-IoT critical environmental testing, and select the most suitable filter types for further simulations. Figure 5.1 shows a BER comparison for NB-IoT with different filter types under the worst-case scenario, 64QAM LTE 12 dB over the optimum power level.

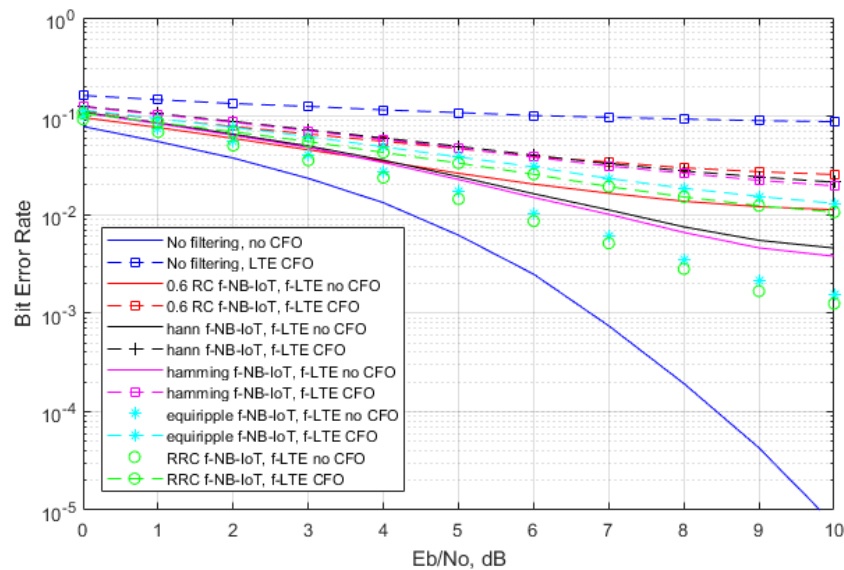


Figure 5.1 NB-IoT BER performance comparison with different filter types under 64QAM critical power level case. 0.6 RC means Huawei proposed 0.6 powered raised cosine filter. CFO testing: NB-IoT synchronized and LTE has 0.5 SC frequency offset.

From the results of this NB-IoT critical power testing case, we can see that windowed sinc method filter is inferior to equiripple filter and RRC filter performance in the in-band NB-IoT mode. Therefore, we select RRC and equiripple filters for more complete simulation studies.

5.1.1 RRC filter

In this simulation scenario, we use root raised cosine (RRC) filter for both NB-IoT and LTE signals. The RRC filter transition band is symmetric around 5×15 kHz, transition bands $5 \times 15 \pm k \times 7.5$ kHz. In our testing, k ranges from 1 to 3, and uses different k values for NB-IoT and LTE.

In general, the RRC filtered NB-IoT signal's PAPR curves (see Figure 5.2) show reduced probabilities for up to about 4.6 PAPR, while the probabilities for higher PAPR's are considerably increased and this increase is higher with small roll-offs. It can be expected that the PA design is somewhat more relaxed in the RRC filtering cases, but more detailed studies would be needed to verify this conclusion.

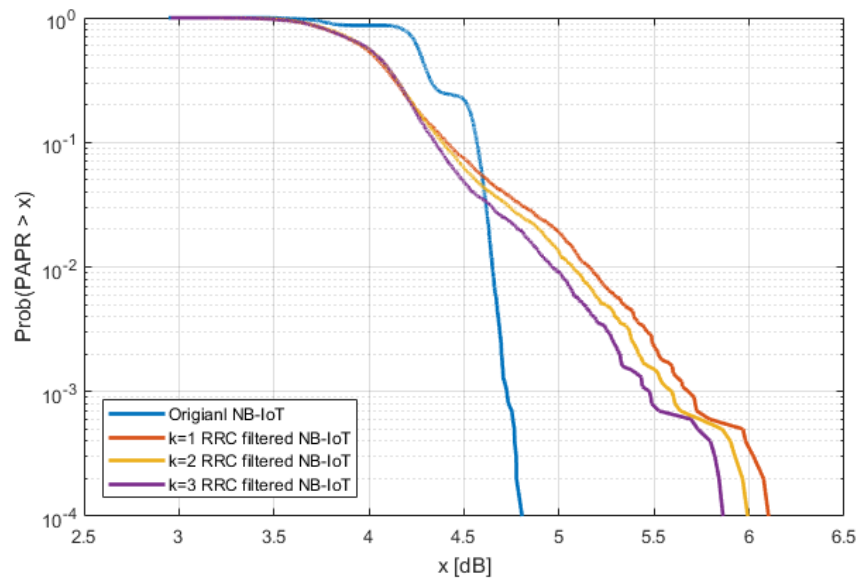


Figure 5.2 PAPR comparison of RRC filtered NB-IoT with different transition bandwidths.

From the error-rate performance results of Figure 5.3 and Figure 5.4, we conclude that sub-band filtering effectively reduces the interference leakage between NB-IoT and LTE, when the system is in the presence of severe CFO. Compared to the reference case (no synchronization errors, no filtering), the performance loss at 1 % BER level is in the order of 1 dB or less, except for the critical test cases with 64QAM. In this scenario and LTE-critical test case (Figure 5.4 (d)), the LTE performance loss is about 2 dB, while in the NB-IoT critical test case (Figure 5.3 (d)), the NB-IoT performance loss is quite significant.

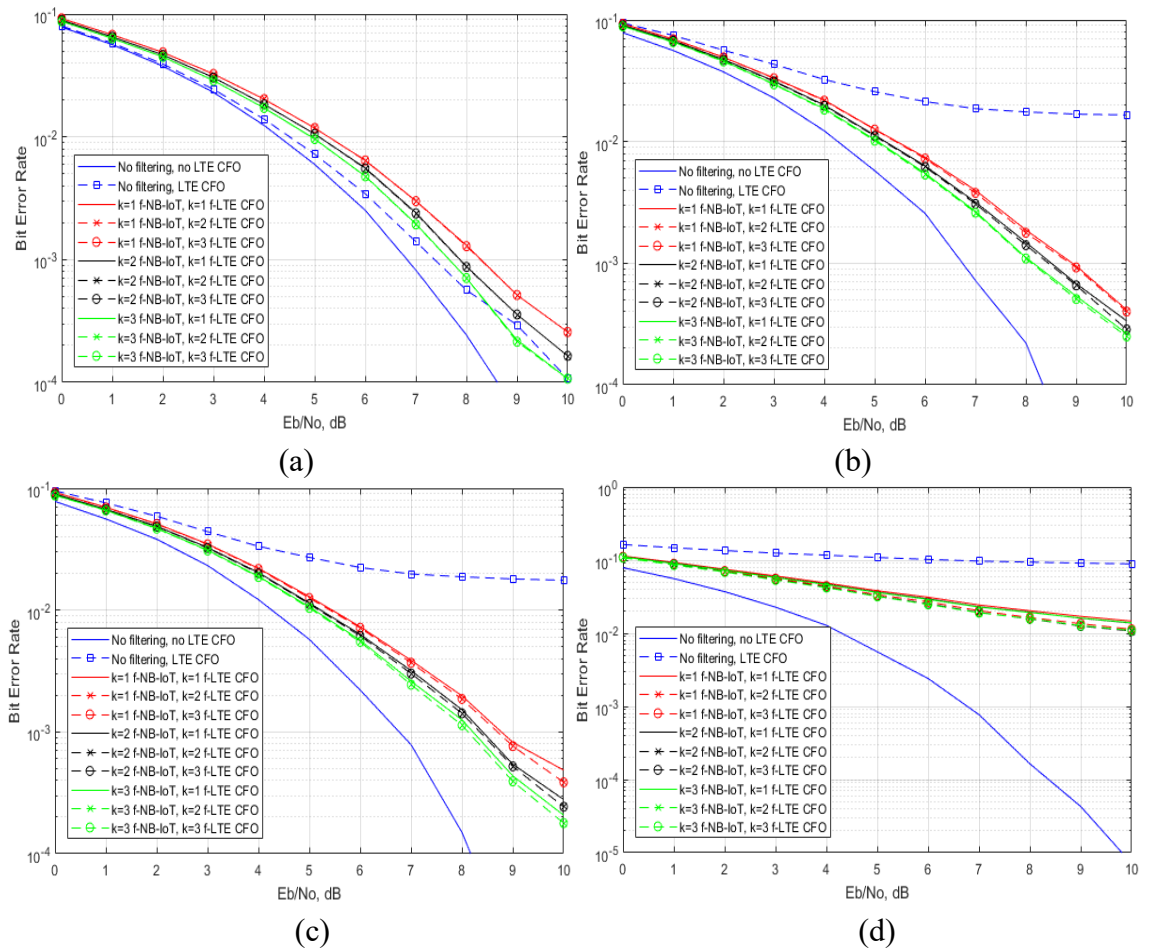
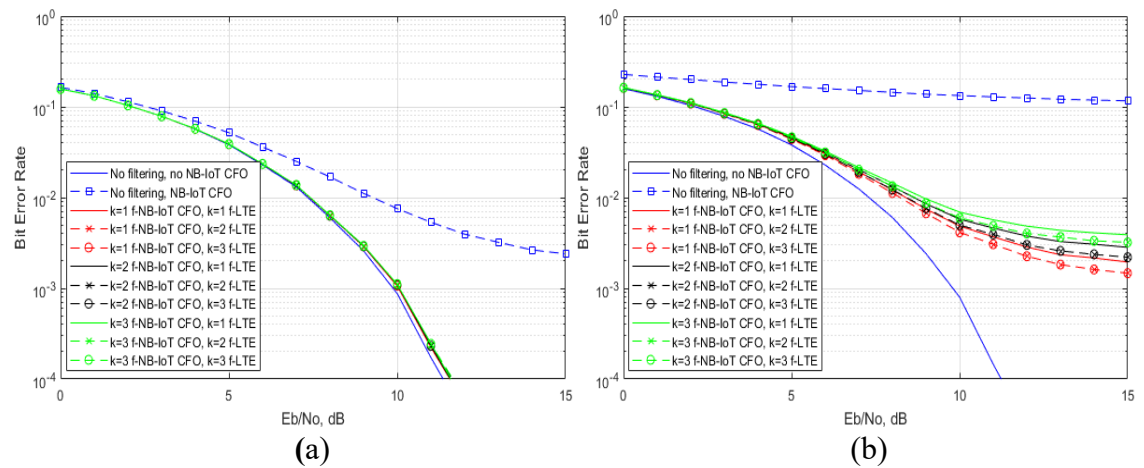


Figure 5.3 NB-IoT CFO error tolerance comparison based on different RRC filter designs. NB-IoT synchronized transmission and LTE with 0.5 SC CFO. (a) 4QAM at optimum power level. (b) 4QAM with 12 dB over optimum power level. (c) 64QAM at optimum power level. (d) 64QAM with 12 dB over optimum power level.



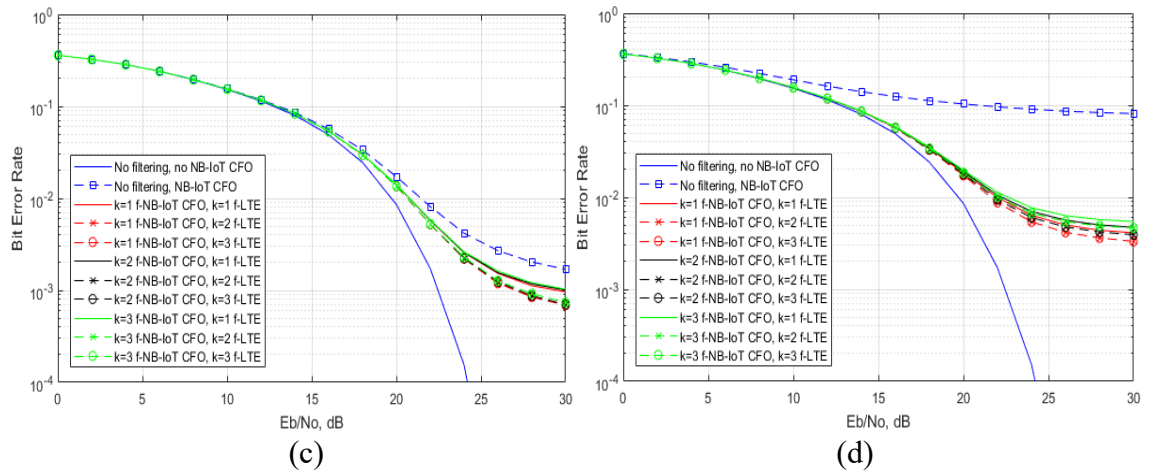
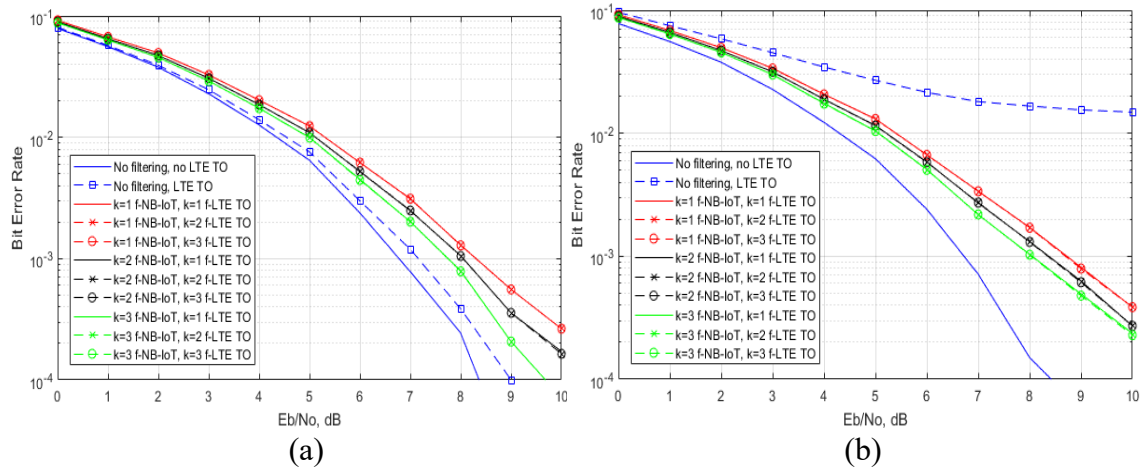


Figure 5.4 LTE CFO errors tolerance comparison based on different RRC filter designs. LTE synchronized transmission and NB-IoT with 0.5 SC CFO. (a) LTE with 4QAM; NB-IoT at optimum power level. (b) LTE with 4QAM; NB-IoT 12 dB over optimum power level. (c) LTE with 64QAM; NB-IoT at optimum power level. (d) LTE with 64QAM; NB-IoT 12 dB over optimum power level.

Regarding the effect of the roll-off of the RRC filter, as the roll-off (k -value) increases, and the NB-IoT capability is slightly improved, but LTE capability is slightly reduced. Next, we check timing offset capability.

We can see that Figure 5.5 and Figure 5.6 TO testing results resemble CFO results. The tolerance of timing error is dramatically improved, especially when the power difference of interference source is large. In addition, the different k value has slightly difference in LTE TO testing.



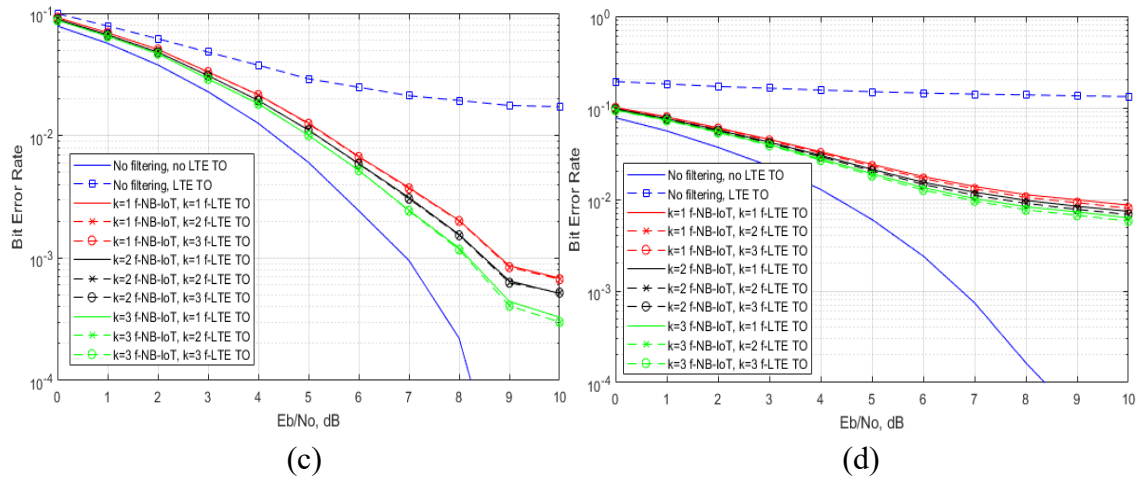


Figure 5.5 NB-IoT TO error tolerance comparison based on different RRC filter designs. NB-IoT synchronized transmission and LTE with 0.5 symbol duration TO. (a) 4QAM at optimum power level. (b) 4QAM with 12 dB over optimum power level. (c) 64QAM at optimum power level. (d) 64QAM with 12 dB over optimum power level.

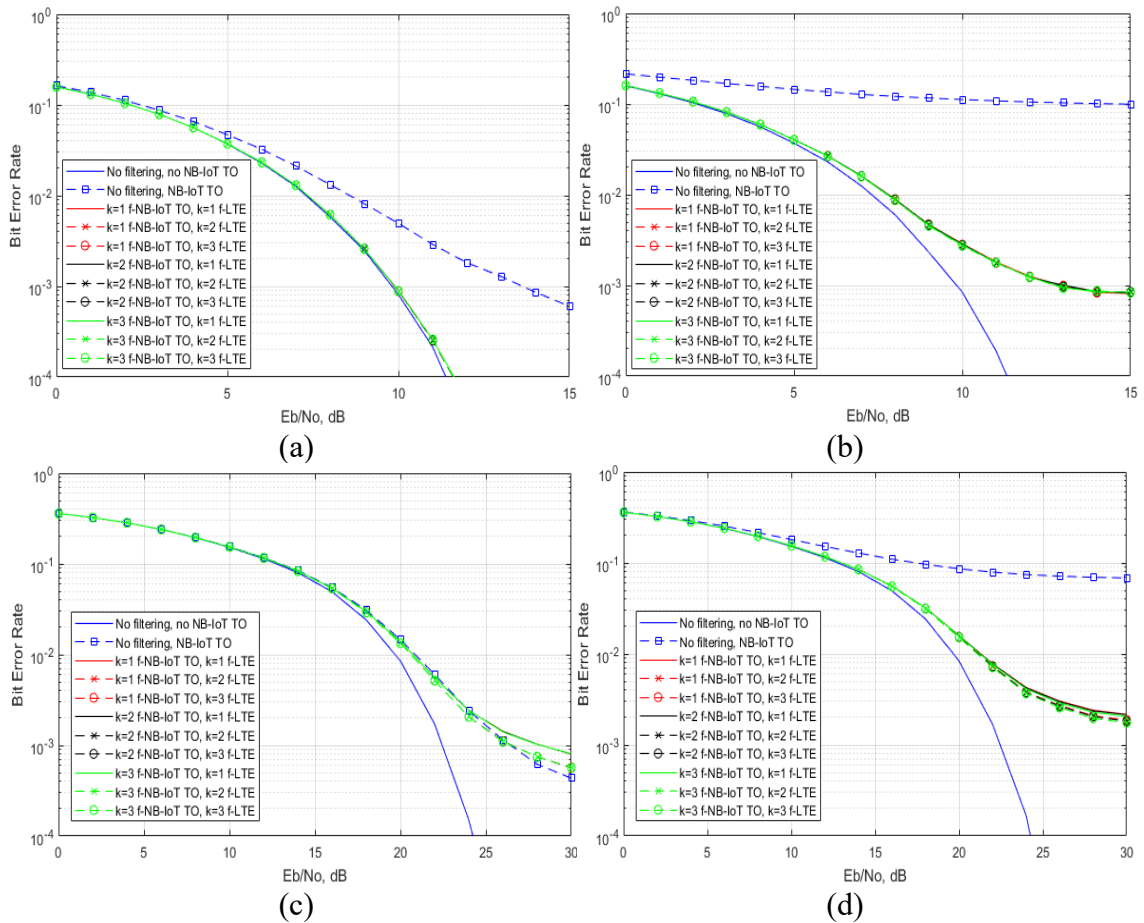


Figure 5.6 LTE TO errors tolerance comparison based on different RRC filter designs. LTE synchronized transmission and NB-IoT with 0.5 symbol duration timing offset. (a) LTE with 4QAM; NB-IoT at optimum power level. (b) LTE with 4QAM; NB-IoT 12 dB over optimum power level. (c) LTE with 64QAM; NB-IoT at optimum power level. (d) LTE with 64QAM; NB-IoT 12 dB over optimum power level.

5.1.2 Equiripple filter

We consider a fairly narrow transition band in equiripple filter design, like 2 to 3 subcarriers with different combinations. In the following results like [4, 6], which denotes the filter with a 4*15 kHz passband edge and 6*15 kHz stopband edge. Firstly, we have a check of CFO effects with different filter configurations.

Figure 5.7 exhibits the PAPR curves of equiripple filtered NB-IoT signal. Although all the filtered cases increase the probability of high PAPR, [5,7]-case presents a mild trend. In this case, there is no active subcarriers localized at transition band.

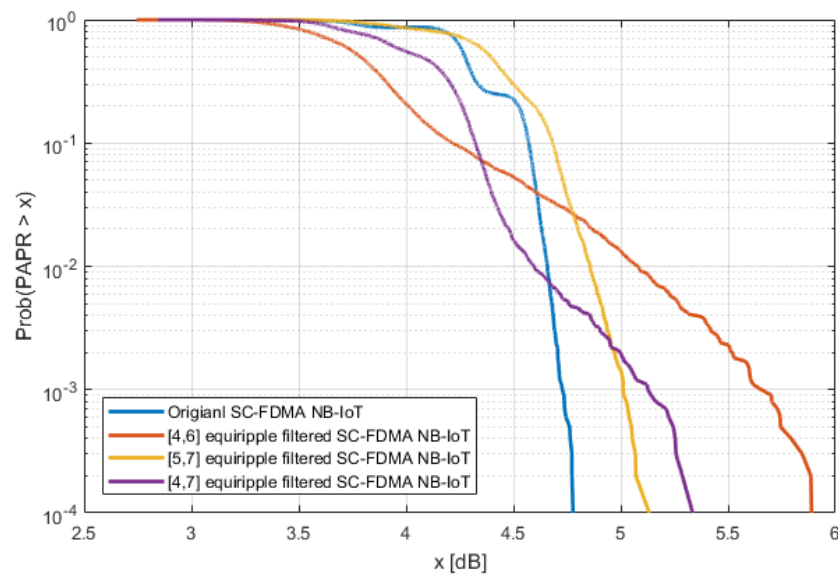
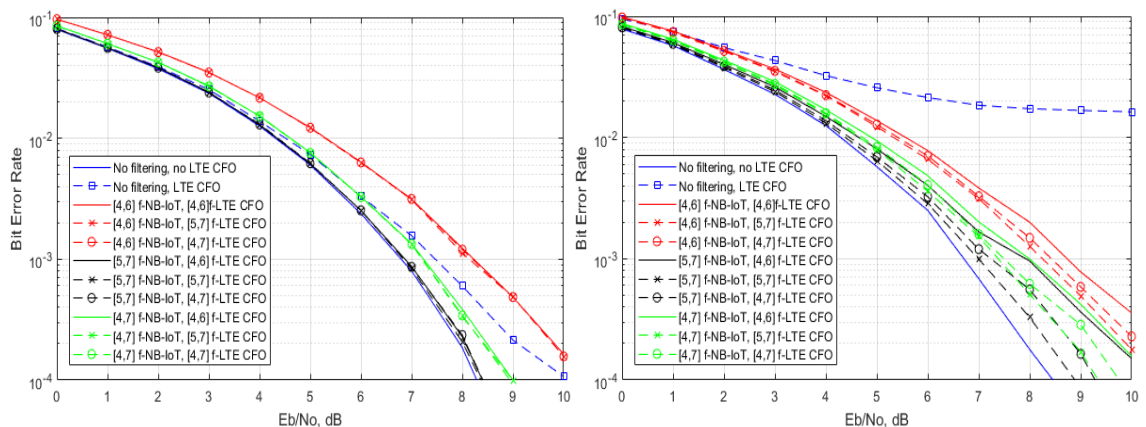


Figure 5.7 Equiripple filtered NB-IoT with various transition bandwidth PAPR comparison.

From the Figure 5.8 and Figure 5.9 testing results, we found that the equiripple filter characteristic is similar to RRC filter. Overall, the 60 kHz passband edge and 90 kHz stopband edge filter configuration is more suitable for critical power control scenario. Next, we examine the filtered system capability in timing offset.



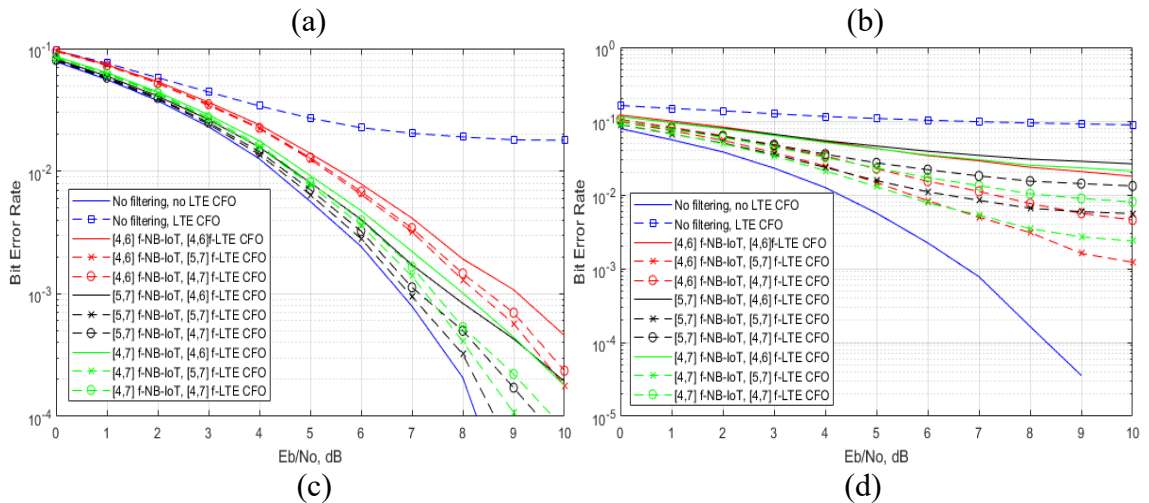


Figure 5.8 NB-IoT CFO error tolerance comparison based on mixed equiripple filter designs. NB-IoT synchronized transmission and LTE with 0.5 SC CFO. (a) 4QAM at optimum power level. (b) 4QAM with 12 dB over optimum power level. (c) 64QAM at optimum power level. (d) 64QAM with 12 dB over optimum power level.

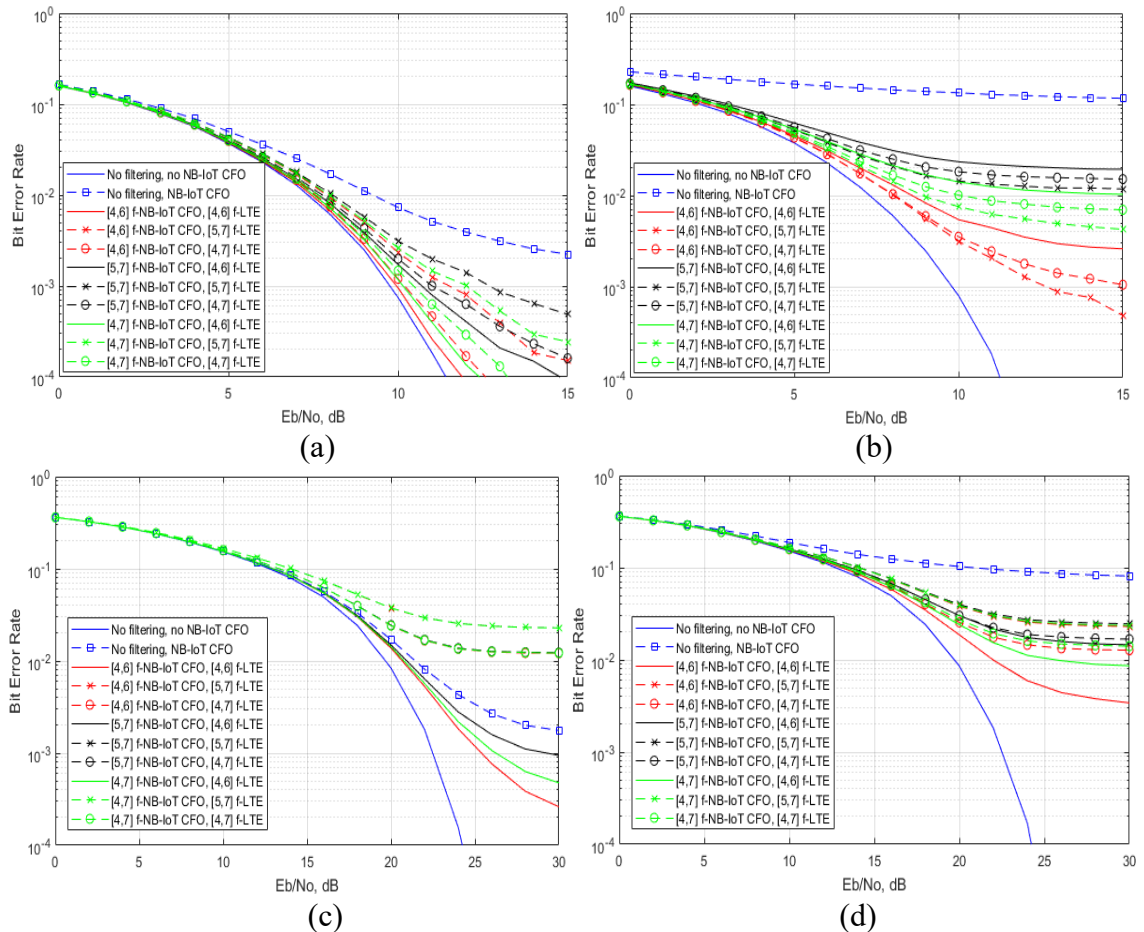


Figure 5.9 LTE CFO error tolerance comparison based on different equiripple filter designs. LTE synchronized transmission and NB-IoT with 0.5 SC CFO. (a) LTE with 4QAM; NB-IoT at optimum power level. (b) LTE with 4QAM; NB-IoT 12 dB over optimum power level. (c) LTE with 64QAM; NB-IoT at optimum power level. (d) LTE with 64QAM; NB-IoT 12 dB over optimum power level.

Figure 5.10 and Figure 5.11 display the equiripple-filter filtered system TO error tolerance results. At 1 % BER level, the filtered system performance loss is in the order of 1 dB or less, compared to the reference case. But, sub-band filtering effectively improves the system capability in the existence of severe TO.

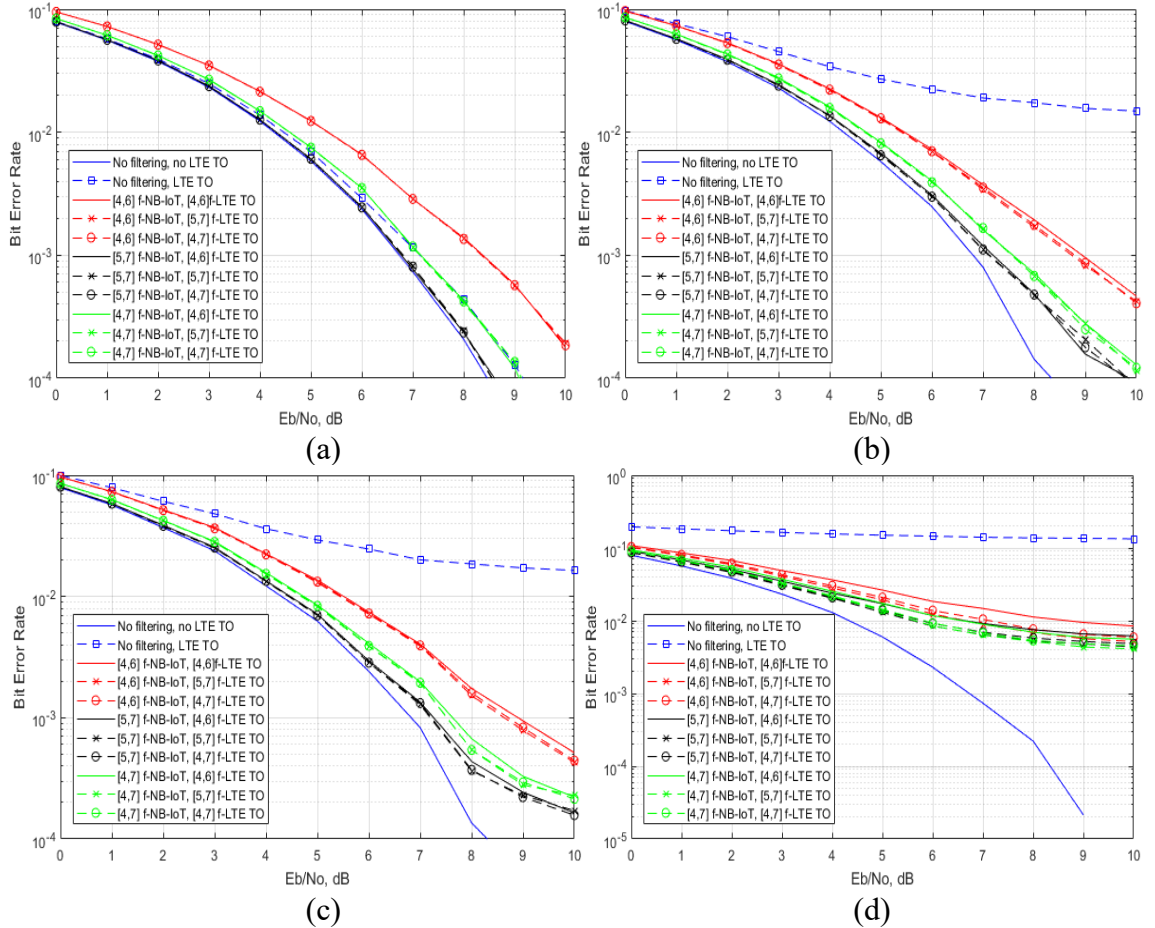
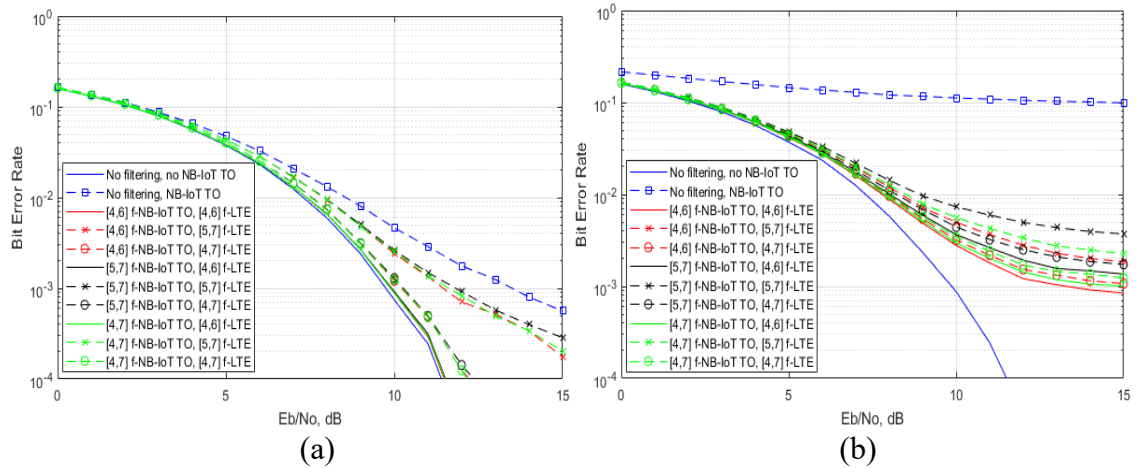


Figure 5.10 NB-IoT TO error tolerance comparison based on different equiripple filter designs. NB-IoT synchronized transmission and LTE with 0.5 symbol duration TO. (a) 4QAM at optimum power level. (b) 4QAM with 12 dB over optimum power level. (c) 64QAM at optimum power level. (d) 64QAM with 12 dB over optimum power level.



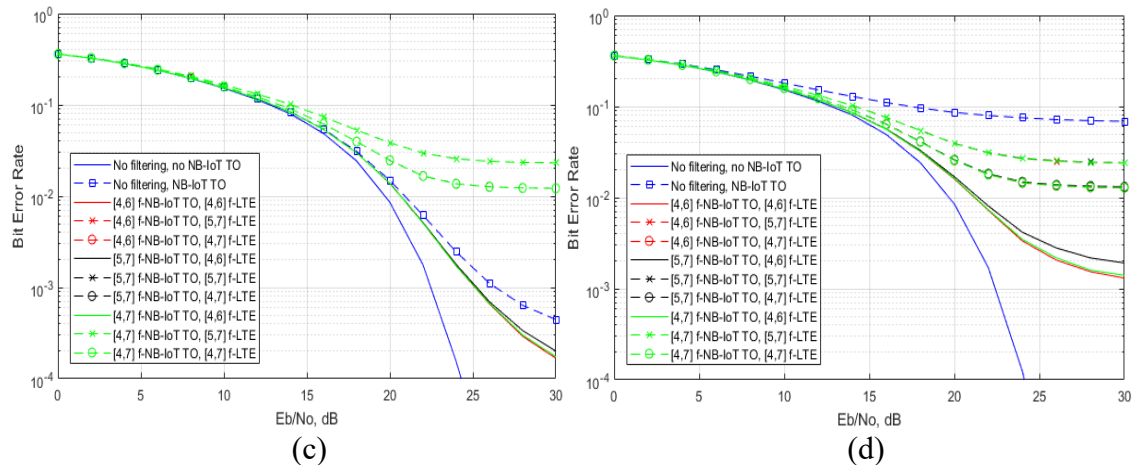


Figure 5.11 LTE TO error tolerance comparison based on different equalripple filter designs. LTE synchronized transmission and NB-IoT with 0.5 symbol duration timing offset. (a) LTE with 4QAM; NB-IoT at optimum power level. (b) LTE with 4QAM; NB-IoT 12 dB over optimum power level. (c) LTE with 64QAM; NB-IoT at optimum power level. (d) LTE with 64QAM; NB-IoT 12 dB over optimum power level.

5.2 Veh-A channel testing

In previous simulation, we find that 4*15 kHz to 6*15 kHz transition bandwidth has a good overall performance. In the following testing scenario with frequency-selective channel, we just test the [4, 6] RRC filter for the system model that contains the Veh-A channel model. In practice, the NB-IoT and LTE user's data reaches base station in uplink through independent channels. Therefore, different channel instances are used for NB-IoT and LTE signals.

Experimental results (see Figure 5.12 and Figure 5.13) exhibit that the channel frequency selectivity degrades the detection performance, thus, we need to increase the E_b/N_o (SNR) to obtain relatively reliable detection results. As a whole, the filtered system shows robustness to worst-case timing and frequency offsets, even under non-ideal power control. The CFO effect is somewhat stronger than the TO effect. The performance can be found to be acceptable, except for the NB-IoT critical and LTE critical test cases with 64QAM modulation, especially with the worst-case CFO.

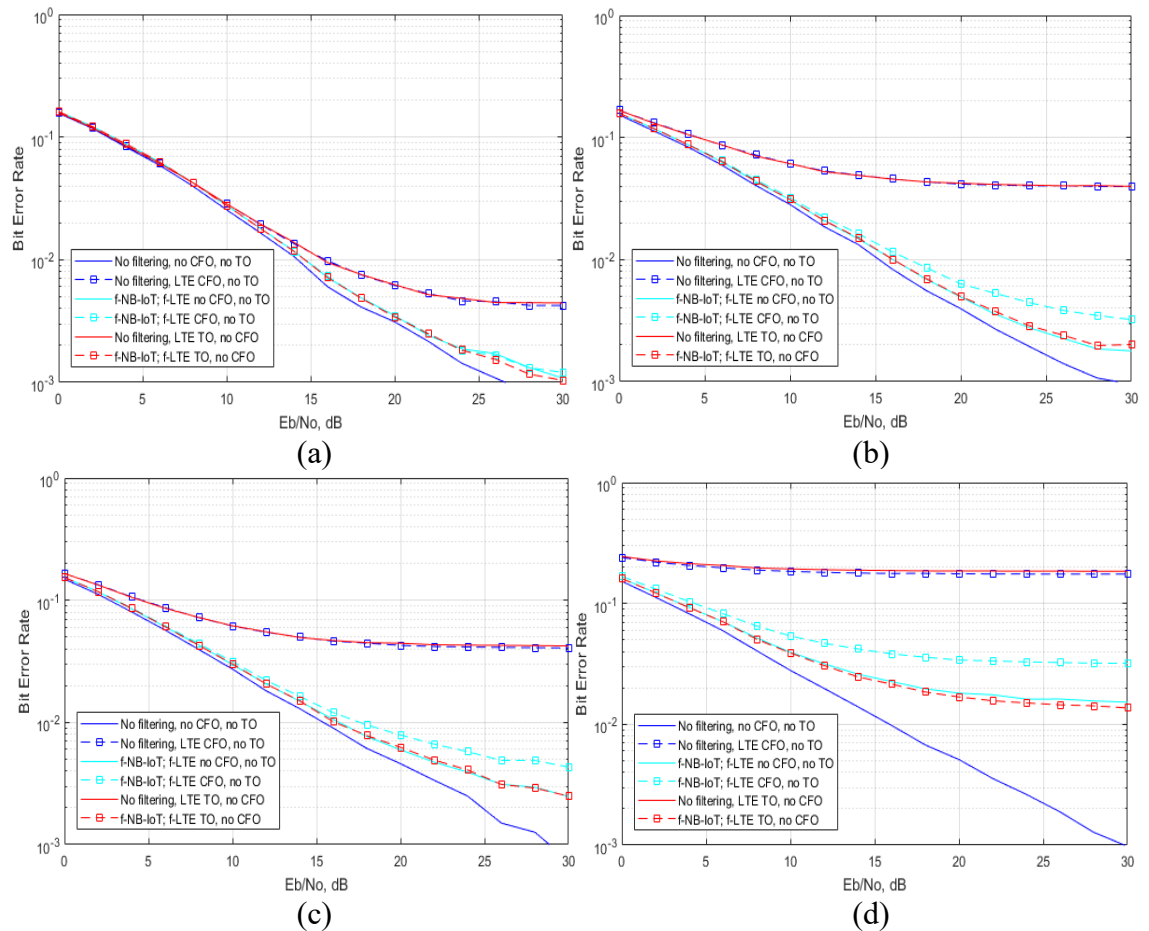
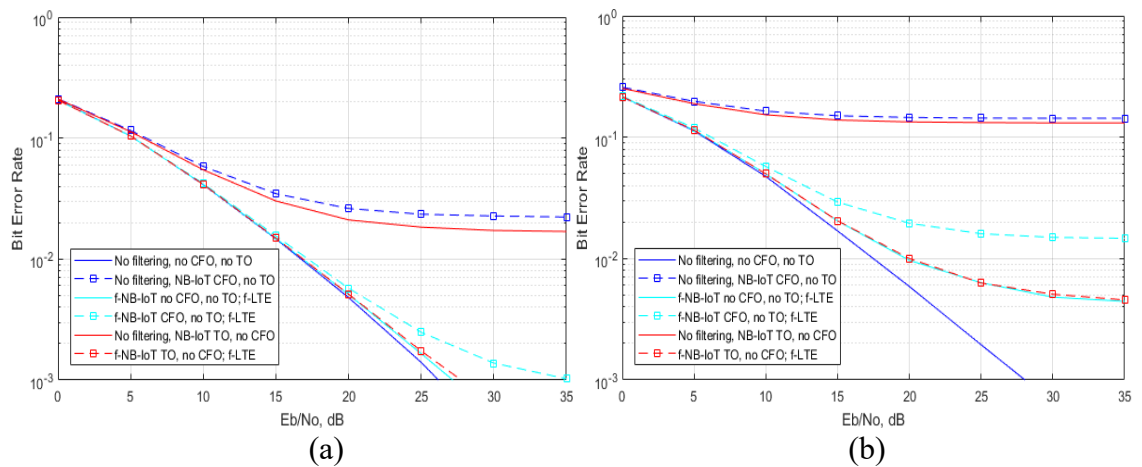


Figure 5.12 NB-IoT error tolerance comparison based on $k=2$ RRC filter design. NB-IoT synchronized transmission and LTE with 0.5 SC CFO or 0.5 symbol duration TO. (a) 4QAM at optimum power level. (b) 4QAM with 12 dB over optimum power level. (c) 64QAM at optimum power level. (d) 64QAM with 12 dB over optimum power level.



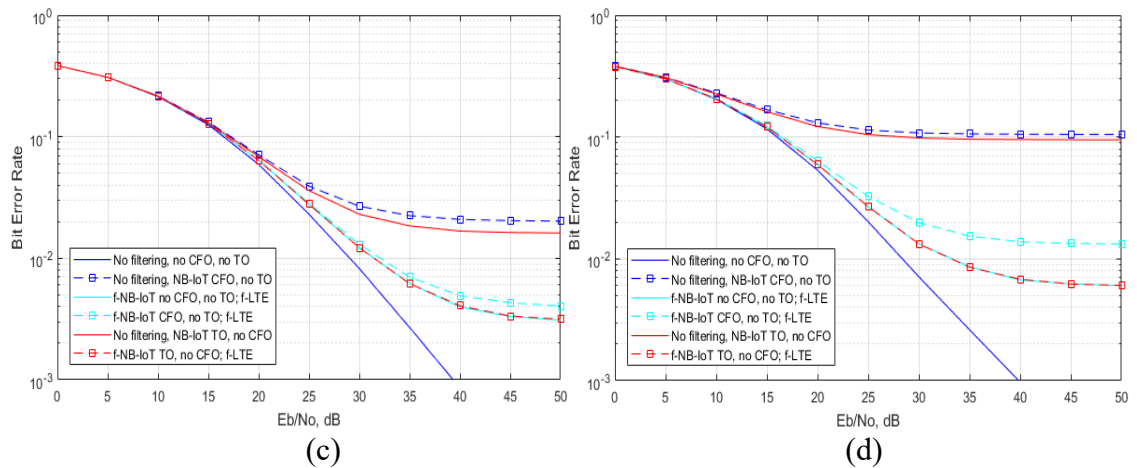


Figure 5.13 LTE error tolerance comparison based on $k=2$ RRC filter design. LTE synchronized transmission and NB-IoT with 0.5 SC CFO or 0.5 symbol duration TO. (a) LTE with 4QAM; NB-IoT at optimum power level. (b) LTE with 4QAM; NB-IoT 12 dB over optimum power level. (c) LTE with 64QAM; NB-IoT at optimum power level. (d) LTE with 64QAM; NB-IoT 12 dB over optimum power level.

6. CONCLUSION AND FUTURE WORK

6.1 Conclusion

Based on a new generation of cellular Internet of Things technology, this thesis focuses on NB-IoT in-band mode enhancement. By changing the fundamental waveform, the out-of-band leakage of each sub-band is significantly restrained. The experimental part mainly includes filter designing, sub-band filtered processing, critical case testing, etc. The main contributions and conclusions of this thesis can be summarized as follows:

1. The structure of the f-OFDM system was investigated, and the feasibility of its application in the NB-IoT system was analyzed. Considering the limited in-band resources, NB-IoT filter needs a fairly narrow transition bandwidth. Moreover, the transition band of the LTE filter cannot affect its active subcarriers, that is, it should span NB-IoT reserved resources. The high PAPR problem of f-OFDM waveform was mitigated by $\pi/2$ -BPSK modulation.
2. The filtered system error-rate performance was evaluated, in the imperfect alignment and non-ideal power control scenarios. Although the filtered waveform slightly degrades ideal system capability, it significantly increases the system robustness to CFO and TO with a high interference power level. This means that asynchronous transmission is supported.
3. The capability of the filtered system in multipath propagation was validated. The frequency selective fading of the ITU-R Vehicular-A channel does reduce the received signal energy such that we need to increase the SNR scale (over 20 dB) to obtain reliable demodulation data. The CFO effect is somewhat stronger than the TO effect.

6.2 Future work

According to previous discussion and analysis of the filtered system, we will do further research on the following aspects:

1. The complexity of the implementation is mainly affected by the filter length, so we can use frequency-domain filtering to reduce the computational complexity.
2. Simulate generic model with NB-IoT deployed in any PRB of LTE, and the low-pass filter designed in this thesis needs to be shifted to the appropriate location as a band-pass filter.
3. Study low complexity PAPR suppression algorithms.
4. Combine LabVIEW and USRP for hardware simulation. Build in-band operation mode and verify the spectral characteristics of filtered signal in the actual system. Test the PAPR characteristics of the transmitted signal.

REFERENCES

- [1] Zanella, A., Bui, N., Castellani, A., Vangelista, L. & Zorzi, M. (2014). Internet of Things for Smart Cities, *IEEE Internet of Things Journal*, Vol. 1(1), pp. 22-32.
- [2] Beyene, Y.D., Jantti, R., Tirkkonen, O., Ruttik, K., Iraj, S., Larmo, A., Tirronen, T. & Torsner, a.J. (2017). NB-IoT Technology Overview and Experience from Cloud-RAN Implementation, *IEEE Wireless Communications*, Vol. 24(3), pp. 26-32.
- [3] Ratasuk, R., Vejlgaard, B., Mangalvedhe, N. & Ghosh, A. (2016). NB-IoT System for M2M Communication, *IEEE Wireless Communications and Networking Conference*.
- [4] Yang, W., Hua, M., Zhang, J., Xia, T., Zou, J., Jiang, C. & Wang, M. (2017). Enhanced System Acquisition for NB-IoT, *IEEE Access*, Vol. 5, pp. 13179-13191.
- [5] Rohde & Schwarz. (2016). 5G Waveform Candidates. Application Note 1MA271
- [6] Zhang, X., Jia, M., Chen, L., Ma, J. & Qiu, J. (2015). Filtered-OFDM - Enabler for Flexible Waveform in The 5th Generation Cellular Networks, *IEEE Global Communications Conference (GLOBECOM)*.
- [7] Abdoli J., Jia M., Ma J. (2015). Filtered OFDM: A New Waveform for Future Wireless Systems, *IEEE International Workshop Signal Processing Advances in Wireless Communications (SPAWC)*.
- [8] Li, J., Bala, E. & Yang, R. (2014). Resource block Filtered-OFDM for Future Spectrally Agile and Power Efficient Systems, *Physical Communication*, Vol. 11, pp. 36-55.
- [9] Terry, J. & Heiskala, J. (2001; 2002). *OFDM wireless LANs: a Theoretical and Practical Guide*, First ed., SAMS, Indiana (IN).
- [10] Myung, H.G. (2007). Introduction to single carrier FDMA, *IEEE European Signal Processing Conference*.
- [11] Dawaliby, S., Bradai, A. & Pousset, Y. (2017). Scheduling Optimization for M2M Communications in LTE-M, *IEEE International Conference on Consumer Electronics (ICCE)*.
- [12] Renfors, M., Yli-Kaakinen, J., Levanen, T., Valkama, M., Ihalainen, T. & Vihriälä, J. (2015). Efficient Fast-Convolution Implementation of Filtered CP-

OFDM Waveform Processing for 5G, IEEE Global Communications Conference (GLOBECOM).

- [13] Press Release. (2017). Cisco Mobile Visual Networking Index (VNI) Forecast Projects 7-Fold Increase in Global Mobile Data Traffic from 2016-2021.
- [14] Moyer B. (2015). A Survey of Longer-Range IoT Wireless Protocols, *Electronic Engineering Journal*.
- [15] Elnashar A. (2015). Building IoT Networks for Smart City, Forum on Internet of Things: Empowering the New Urban Agenda, Geneva, Switzerland.
- [16] Kopp, J. (2016). NB-IoT and eMTC Make 4G Networks Ready for the Internet of Things, *Microwave Journal*, Vol. 59(11), pp. S20.
- [17] Qualcomm. (2017). LTE IoT is Starting to Connect the Massive IoT Today, thanks to eMTC and NB-IoT.
- [18] Bashore, F. (2000). OFDMs for Wireless Multimedia Communications, *Microwave Journal*, Vol. 43(8), pp. 178.
- [19] Wang, Y., Lin, X., Adhikary, A., Grovlen, A., Sui, Y., Blankenship, Y., Bergman, J. & Razaghi, H.S. (2017). A Primer on 3GPP Narrowband Internet of Things, *IEEE Communications Magazine*, Vol. 55(3), pp. 117-123.
- [20] 3GPP TR 45.820 V2.1.0. (2015). Cellular System Support for Ultra Low Complexity and Low Throughput Internet of Things.
- [21] 3GPP TS 36.101 V13.4.0. (2016). User Equipment (UE) radio transmission and reception.
- [22] 3GPP TS 25.300 V13.0.0. (2016). Universal terrestrial radio access network.
- [23] 3GPP TS 36.211 V13.2.0. (2016). Physical channels and modulation
- [24] 3GPP TR 36.888 V.12.0.0. (2013). Study on Provision of low-cost Machine-Type Communications (MTC) User Equipments (UEs) based on LTE.
- [25] Rohde & Schwarz. (2016). Narrowband Internet of Things Whitepaper.
- [26] 3GPP R1-161448. (2016). WF on DM-RS design for PUSCH.
- [27] 3GPP R1-1613597. (2016). WF on $\pi/2$ BPSK Modulation (Additional low PAPR Technique).

- [28] 3GPP R1-1704782. (2017). $\pi/2$ BPSK with Precoding/Post-DFT Subcarrier Spectrum Shaping.
- [29] Banelli, P. & Cacopardi, S. (2000). Theoretical Analysis and Performance of OFDM Signals in Nonlinear AWGN Channels, *IEEE Transactions on Communications*, Vol. 48(3), pp. 430-441.
- [30] Pauluzzi, D.R. & Beaulieu, N.C. (2000). A Comparison of SNR Estimation Techniques for the AWGN Channel, *IEEE Transactions on Communications*, Vol. 48(10), pp. 1681-1691.
- [31] Henkel, W., Taubock, G., Odling, P., Borjesson, P.O. & Petersson, N. (2002). The Cyclic Prefix of OFDM/DMT - an Analysis, *IEEE International Zurich Seminar on Broadband Communications Access - Transmission - Networking* (Cat. No.02TH8599).
- [32] Van Eeckhaute, M., Bourdoux, A., De Doncker, P. & Horlin, F. (2017). Performance of Emerging Multicarrier Waveforms for 5G Asynchronous Communications, *EURASIP Journal on Wireless Communications and Networking*, Vol. 2017(1), pp. 1-15.
- [33] 3GPP TR 36.888. (2013). Study on Provision of low-cost Machine-Type Communications (MTC) User Equipments (UEs) based on LTE.
- [34] 3GPP R1-166999. (2016). Detailed Configuration of f-OFDM and W-OFDM for LLS evaluation.
- [35] 3GPP R1-165425. (2016). f-OFDM Scheme and Filter Design.
- [36] 3GPP R1-162199. (2016). Waveform Candidates.
- [37] Ohno, S. & Teo, K.A.D. (2007). Universal BER Performance Ordering of MIMO Systems Over Flat Channels, *IEEE Transactions on Wireless Communications*, Vol. 6(10), pp. 3678-3687.
- [38] Pandey, D. & Dewangan, N. (2015). Performance analysis of pilot assisted channel estimation in OFDM, *IEEE International Conference on Computer, Communication and Control (IC4)*.
- [39] Nosrat-Makouei, B., Yazdan-Panah, A. & Vaughan, R.G. (2007). Pilot Feedback Equalization for Time Varying OFDM Systems, *IEEE Canadian Conference on Electrical and Computer Engineering*.